A numerical study of ammonia dispersion in an industrial area with the CFD tool FLACS

Rebecca Kjørsvik-Abbedissen

A thesis submitted in partial fulfilment of the
requirements for the degree of Master of Science in
the subject of *Process Safety Technology*

Department of Physics and Technology
University of Bergen
Bergen, Norway
June 2018

Acknowledgement

As a start I would like to thank my supervisor, Associate Professor Bjørn J. Arntzen for facilitating and introducing me to this thesis. His time, patience and feedback throughout this process has played a great role in the outcome.

Next, to the kind and encouraging people I have had the pleasure of sharing an office with; thank you. Thank you for joining me in brainstorming and discussions, and offering kind and motivational words. I would have never managed this with you.

Last but not least, I would like to thank my amazing family and friends, who has offered their time and company to help me get through this period.

Bergen, 1 June 2018

Rebecca Kjørsvik-Abbedissen

Abstract

As the use of ammonia increases, knowledge about dispersion patterns and dispersion tendencies is of enhanced importance. Due to its toxic nature, very few realistic experiments of ammonia dispersion in complex situations have been completed, and one has to rely on numerical models instead. Many of these models are traditional, simplified dispersion models, which are not valid in complex situations. Therefore, CFD (Computational Fluid Dynamics) codes, such as FLACS, are essential. The codes are in constant development, and new models that comprehend new scenarios are regularly added. In this thesis, release and dispersion of ammonia in a complex industrial area is studied. By varying wind speed and wind direction, different scenarios are produced and examined. The varying wind conditions are found to result in a range of dispersion patterns, where the distance covered on land vary from 72 m to 1660 m. Due to the extensive dispersion in some scenarios, and accompanied enlarging of the considered domain, the grid cells had to be adjusted to maintain an acceptable computational time. This seemingly brings by an overestimation of the extent due the implementation of larger cells. The effects of changing the temperature or adding a Pasquill class is not remarkable, while elevating the leak or removing the obstacles result in a completely different dispersion.

Contents

Nomenclature

Latin symbols

$\boldsymbol{a}$	Acceleration	$\mathrm{m \cdot s^{-2}}$
C_p	Heat capacity	$\mathrm{J \cdot mol^{-1}K^{-1}}$
f	Body force	$\mathrm{N \cdot m^{-3}}$
$\boldsymbol{F}$	Force	N
h	Standard enthalpy	$\mathrm{J \cdot mol^{-1}/J \cdot kg^{-1}}$
k	Turbulent kinetic energy	$\mathrm{J \cdot kg^{-1}}$
m	Mass	kg
M	Molecular weight	$\mathrm{g \cdot mol^{-1}}$
p	Pressure	Pa
R	Ideal gas constant ≈ 8.314	$\mathrm{J \cdot K^{-1}mol^{-1}}$
t	Temperature/1000	°C/K
t	Time	s
T	Temperature	°C/K/R
$\boldsymbol{u}$	Velocity vector	$\mathrm{m \cdot s^{-1}}$
u	Wind speed	$\mathrm{miles \cdot hour^{-1}}$
VP	Vapor pressure	psia
z_0	Roughness length	m

Greek symbols

ε	Mean height of roughness objects	m
ε	Rate of turbulent kinetic energy dissipation	$\mathrm{J \cdot kg^{-1}s^{-1}}$
ρ	Density	$\mathrm{kg \cdot m^{-3}}$
τ	Shear and normal stress	Pa

Other symbols

∂	Partial derivative
$\nabla\cdot$	Divergence
$\equiv$	Definition

Abbreviations

AEGL	Acute Exposure Guideline Levels
CASD	Computer Aided Scenario Design
CFC	Chlorofluorocarbon
CFD	Computational Fluid Dynamics
DNS	Direct Numerical Simulation
FLACS	FLame ACceleration Simulator
IDLH	Immediately Dangerous to Life or Health
IIAR	International Institute of Ammonia Refrigeration
LES	Large Eddy Simulation
LFL	Lower Flammable Limit
LNG	Liquid Natural Gas
MEP	Model Evaluation Protocol for LNG vapor dispersion models
MIE	Minimum Ignition Energy
NIOSH	National Institute of Safety and Health
ppm	Parts per million
RANS	Reynolds-Averaged Navier Stokes
UFL	Upper Flammable Limit

Chapter 1

Introduction

1.1 Motivation

Every year we see several accidental releases of ammonia, occurring from very different storage conditions, and with varying size and consequence. Common to the ammonia storage units is that they often store substantial quantities, which greatly increases the potential of injury in the case of a release.

In 2002 one person and 170 animals lost their lives when an ammonia tank exploded at a farm in Larvik, Norway, and led to dispersion of the gas [1]. A more recent incident happened in Shanghai, China in 2013, where a detached pipe cap lead to liquid ammonia being spread and the gas dispersing at a refrigeration facility. As a consequence 15 people were killed and 25 were injured, whereas six of them suffered critical injuries [2].

One of the key problems when it comes to intentional or accidental releases of toxic substances, such as ammonia, is to be able to predict the dispersion and concentration distribution obtained. Facilities storing ammonia are subject to laws and regulations, which has led to most facilities having the required alarm systems and emergency ventilation in place. If these systems meet the requirements, the facility should be able to detect releases quickly and the ventilation should lead to flushing of the release location and affected areas in a satisfactory manner. However, if this is a fact, the released gas could end up dispersing to vital and vulnerable areas in the near vicinity of the facility, leading to a shift of exposure risk to these areas.

Assessing accidental releases and preventing them is an important part of the risk analysis conducted by the facilities handling and utilizing ammonia. As well as assessing the risk inflicted on the workers involved, it is vital to assess the risk for third parties, such as the community surrounding the facility. Early detection is key to stop an ongoing leak, but once the leak has occurred, knowledge about the way the gas will disperse according to the current wind speed and direction is of critical importance. Will the gas reach surrounding areas? Will the gas be diluted before it reaches any vital locations? Are certain areas more affected than others?

In the case of an emergency evacuation due to a release, the evacuation of the assumed affected areas are today based on simple dispersion models, due to the lack of other sources. These models often conclude with circular evacuation areas, where factors such as wind direction are not taken into account. The general guidelines obtained are used independently of the scenario and topography, and can thereby prove to be very conservative or, depending on the conditions, not adequate at all. Thus, a thorough investigation of gas dispersion according to the current topography and actual wind characteristics is required to handle a release in the most efficient and hassle-free way possible.

Examining the risk for ammonia exposure for third parties is becoming of greater importance for an increasing amount of industries as ammonias span of usage broadens. If ammonias abilities as a possible energy carrier is acted upon, it can make ammonia readily available to the average person and information about dispersion will have enhanced importance to improve the knowledge and increase the safety.

1.2 Objective

The objective of this thesis is to simulate dispersion of ammonia at a given location by utilizing the CFD tool FLACS. By varying wind speed and direction, different dispersion scenarios will be produced and analyzed. In this way, a detailed picture of the affected areas in the case of a release is obtained.

Second, the ability of FLACS to simulate release and evaporation of liquid ammonia is tested.

1.3 Previous work

The previous studies completed, either numerical or experimental, have generally focused on combined release and dispersion situations, initially from a liquid state. The common denominator of the experimental studies involving release and dispersion of ammonia is that they are completed in very simple environments far away from humans, often in a desert or in more remote areas. Due to ammonias hazardous nature, experimental dispersion studies of the substance in more complex environments have not yet been completed. For the examination of these scenarios, we rely on the abilities of computational fluid dynamics (CFD), which has proven to be a highly efficient alternative.

Several numerical studies have been conducted on ammonia dispersion where different CFD tools, including FLACS, have been applied. Some of the numerical studies, where FLACS has been chosen as the CFD tool, are described below.

Greulich and Hansen [3] studied the dispersion of ammonia after a release from a relief vent discharging vertically to the atmosphere using FLACS. The setting was an urban area with buildings with varying height and where the highest point in close proximity was the release. Different scenarios were produced by altering the wind speed and direction, and the objective was to measure the concentration of the released gas at street level. The results showed that the by-far highest concentration was found for given wind directions, but the results concerning wind speed were not that prominent.

Gavelli et. al [4] completed a series of simulations of ammonia dispersing in an urban environment consisting of buildings with varying height. The assumed situation was a large breach of the storage tank of a tank truck accompanied by a large release of flashing liquid, in other words, a combination of a liquid pool and gas dispersion. Different dispersion conditions was defined by varying the wind directions, and obstructed dispersion with buildings vs. unobstructed dispersion was also compared. The objective of the study was to prove that the method within emergency preparedness where, when an incident with a hazardous material occurs, and a hazard radius is assigned around the site, could be both conservative and not adequate at all. This was proven, and the enhanced turbulent mixing due to obstructions were well documented for a set of eight wind directions.

Gavelli et. al [5] conducted simulations of the Jack Rabbit I experiments, where pressurized liquefied ammonia and chlorine were released and dispersed. The motivation behind the simulations was to evaluate the ability of FLACS to model dispersion and a two-phase flashing jet. In this blind test, a model for two-phase flow, which at the time of the implementation were

quite new, was put to the test to simulate both the formation of a pool and the accompanied dispersion. For more detailed information about the experiments in Jack Rabbit I, the first of two trials in the Jack Rabbit project, the reader is referred to Storwold et. al [6].

1.4 Outline of the thesis

The next chapter, Chapter 2, presents background information regarding ammonia, factors influencing dispersion, and what CFD and FLACS is all about.

In Chapter 3 the first part of the simulations, pool simulations, is presented, with a walk-through of the setup and results obtained.

Chapter 4 gives a description of the simulations of ammonia dispersion, while a conclusion and recommendations for further work is provided in Chapter 5.

Chapter 2

Background

The current chapter introduces the background required to understand this thesis. Facts and properties about ammonia is presented, as well as why it is considered dangerous when exposed to it. Then, a walkthrough of the factors affecting dispersion is given. The last part of this chapter is about the fundamentals making up computational fluid dynamics (CFD) and information about the certain tool used in this thesis, FLACS.

The intent of this chapter is to provide an overview of the topics. For more details, the reader is referred to the specified references.

2.1 Ammonia

2.1.1 Properties

Ammonia with the chemical formula NH_3 can be found in either a solid, liquid or gaseous state, depending on its pressure and temperature. Both the liquid and gas is considered colorless but is often perceived as a white fog due to the condensation of H_2O in air when it is released to the surroundings. At standard conditions, defined as 1 bar and 0°C, ammonia in its liquid and gaseous states have a lower density then water and air, respectively.

Among its properties, ammonia is especially known for its high thermal conductivity and high heat capacity in both its liquid and gaseous state. These thermodynamic properties lead to ammonia conducting heat very well, especially in situations involving phase change, making it an ideal fluid for, among other things, refrigeration. Research has showed that ammonia is the most desirable fluid for the Rankine cycle, which involves conversion of heat to mechanical work while the fluid undergoes phase change [7].

Some selected physical properties of ammonia are rendered in table 2.1. What can be seen from the table below is that ammonia has a very narrow flammability range. This makes it difficult to achieve a flammable cloud, especially outside, when released from storage. This fact alone leads to ammonia in many instances not being considered a flammable gas and the only aspects considered in the consequence of the dispersion, is its toxicity.

2.1.2 Hazards and Toxicity

Ammonia pose a hazard in the way that it is toxic and can cause burn and irritation to exposed areas of the body, and is corrosive to, and not compatible with, certain materials.

Ammonia, with its distinct smell, is easily recognized, and the lower limit for smelling it is 5 ppm. It is toxic to the body via inhalation and ingestion, and when inhaled, the gas irritates

Table 2.1: Selected physical properties of ammonia rendered from IIAR's *Ammonia databook* [7]. LFL and UFL are given in volume percent of air. Two different sets of values of the flammability limits are specified in IIAR's handbook, but here it is chosen to establish the widest interval as the ruling one, as most recent sources coincide about this interval.

Property	**Condition**	**Value (SI)**
Molecular Weight		17.03 g/mol
Physical State	Room temperature, p = 101325 Pa = 1 atm	Gas
Freezing Point	p = 101325 Pa = 1 atm	-78°C
Boiling Point	p = 101325 Pa = 1 atm	-33.4°C
Critical Pressure		11410 Pa
Critical Temperature		133°C
Lower Flammable Limit (LFL)		15 vol-%
Upper Flammable Limit (UFL)		28 vol-%
Minimum Ignition Energy (MIE)		680 mJ
Odor Threshold		5-50 ppm

the respiratory passages, and particularly the upper airways. Liquid ammonia causes chemical burns when it comes in direct contact with the skin, and the injury will depend on the length of the exposure. The temperature of liquid ammonia at atmospheric pressure is lower than the boiling point at -33°C and thereby also causes cryogenic injuries, contributing to serious tissue damage alongside the chemical burns.

Ammonia is a hydrophilic substance by nature, and thereby especially attacks parts of the body where moisture is often found, like armpits, eyes and the groin. The reaction with H_2O leads to the production of ammonium hydroxide, which is an exothermic chemical reaction. Due to the exothermic properties of the reaction, heat is generated, and the ammonium hydroxide causes necrosis of the tissue: killing of cells [8].

To describe ammonias toxicity, quite a few definitions of boundary values and levels can be found in the literature, with the purpose of acting as guidelines in industry and emergency response situations. Two selected ones are described below.

The term 'immediately dangerous to life or health (IDLH)', developed by the National Institute for Occupational Safety and Health (NIOSH), describes exposure to airborne pollutants and defines levels where, when exposed to higher concentrations, only a highly reliable breathing apparatus is allowed [9]. This value is set to 300 ppm for ammonia. Further, an exposure of 300 to 500 ppm for 30 to 60 minutes has been reported as a maximum short exposure tolerance. For the same time interval, 2500 to 6000 ppm is dangerous to life, while 5000 to 10000 ppm is fatal.

The National Advisory Committee for Acute Exposure Guideline Levels for Hazardous Substances has identified Acute Exposure Guideline Levels (AEGL) for ammonia. Three levels are identified and defined based on a set of criteria, and assigned a value depending on the emergency exposure period, which ranges from 10 minutes to 8 hours. The three levels are all given in parts per million (ppm) or milligrams per cubic meter (mg/m^3) and are defined as follows [10]:

1. AEGL-1: The airborne concentration of ammonia above which the exposed population could experience non-disabling, reversible discomfort or irritation.
2. AEGL-2: The airborne concentration of ammonia above which the exposed population could experience irreversible or other serious long-lasting health effects.
3. AEGL-3: The airborne concentration of ammonia above which the exposed population could experience life-threatening health effects or death.

The defined concentrations at the given levels are listed in table 2.2. When exposed to concentrations lower than the weakest concentration given in the table, discomfort and irritation

in airways and eyes may still be experienced. The degree of irritation and effect will vary from individual to individual depending on physiological differences like age and illness, but as the concentrations increases, the likelihood of experiencing effects rises with it [10].

Table 2.2: Acute Exposure Guideline Levels (AEGL) for ammonia, describing levels of increasing damage at given exposure times [10].

Classification	**Exposure time**				
	10 min	**30 min**	**1 hour**	**4 hours**	**8 hours**
AEGL-1 (non-disabling)	30 ppm (21 mg/m^3)	30 ppm (21 mg/m^3)	30 ppm (21 mg/m^3)	30 ppm (21 mg/m^3)	30 ppm (21 mg/m^3)
AEGL-2 (disabling)	220 ppm (154 mg/m^3)	220 ppm (154 mg/m^3)	160 ppm (112 mg/m^3)	110 ppm (77 mg/m^3)	110 ppm (77 mg/m^3)
AEGL-3 (lethal)	2700 ppm (1888 mg/m^3)	1600 ppm (1119 mg/m^3)	1100 ppm (769 mg/m^3)	550 ppm (385 mg/m^3)	390 ppm (273 mg/m^3)

2.1.3 Use

Ammonia for direct use is largely synthesized through the Haber-Bosch-process, where nitrogen and hydrogen is combined using a catalyst under very high pressure to form ammonia [11]. Even though it is synthesized, it is still considered a natural substance due to its occurrence in organic processes in nature. Most of the ammonia is used for agricultural purposes, such as crop fertilizer, and in the U.S. in 2014, 88% of ammonia consumption was due to fertilizer use [12].

Nitrogen and hydrogen can, as mentioned above, combine to produce ammonia, but ammonia can also be divided into its two constituents and become a source of nitrogen and hydrogen. Nitrogen is a common product in explosives such as TNT and nitroglycerin, and together with ammonia, it makes up ammonium nitrate, which form a very explosive mix when combined with fuel oil. The ammonium nitrate is also a common fertilizer. The hydrogen can further be used in, for instance, fuel cells, and ammonia as a hydrogen carrier makes transportation of hydrogen easier [13].

Ammonia is also a common refrigerant, where ammonia at a weight percent of minimum 99.95% is required. In the refrigeration industry, anhydrous ammonia, i.e. ammonia containing no water, is used, and goes by the name R-717. The use of ammonia as a refrigerant has increased in recent years due to that previous alternatives, especially chlorofluorocarbons (CFCs), has been found to be a big contributor to the depletion of the stratospheric ozone layer, and thereby tremendously harmful to the environment [14]. Ammonia, as the complete opposite, has no ozone depletion or global warming potential, which is very appreciate in today's climate focused society [15]. The low odor threshold, far below any limit for injuries, makes ammonia a relatively safe refrigerant since the fumes alone act as an alarm for the exposed parties.

Set aside from the advantages ammonia prove against alternative refrigerants, ammonia also has a disadvantage. Ammonia is incompatible with different materials containing metals such as copper and zinc, leading to corrosion of these materials [7]. Because of this, the transition from previously used refrigerants, such as freon and CFCs, was in some cases difficult, expensive and inefficient due to large parts of the plant having to be rebuilt with new, compatible materials. However, the resulting rebuild ammonia plant is often smaller when completed, since ammonia requires smaller refrigerant piping than other alternatives [15].

Due to today's society being just that - climate focused - new usages of ammonia is currently being researched and some has already emerged. A fairly new use of ammonia, is the use of

ammonia as fuel, both in fuel cells and as a fuel for transportation. Afif et al. [13] provides a thorough review on different fuel cells fed on ammonia.

The fact that ammonia contains no carbon leads to no production of CO_2 if it is burned, and thereby to it being a good alternative as a fuel if one solely considers CO_2 emissions. However, ammonia, with its MIE of 680 mJ compared to gasolines 0.8 mJ, is difficult to apply directly in a spark ignited internal combustion engine, due to the large amount of energy required to ignite it. This has been studied and it has been shown that when gasoline [16] or hydrogen [17] is mixed with ammonia, it lowers the MIE and leads to good engine performances.

Another fuel containing no carbon and being a seemingly good alternative as a fuel, is hydrogen. Wanting to use hydrogen as a fuel or an energy carrier in general has proven to be difficult and means are needed to help this process along. Among other things, the challenges relate to the storage and distribution of the substance. A quite few metal hydrides have been synthesized and tried as a medium for hydrogen storage but has fallen short when looking at certain wanted properties. As the other carbon-free chemical energy carrier, ammonia has risen to the occasion as a viable option. Ammonia is already well adapted for storage and transportation and as a hydrogen storage alternative it has the advantages of a highly developed infrastructure and process for synthesizing, high hydrogen density, and easy catalytic decomposition [18].

Other usages of ammonia include neutralizing crude oil constituents in the petroleum industry, pre-harvest cotton defoliant, and as pH control in water and waste management. Ammonia is also extremely soluble in water and is thus a very common component in household cleaning products. Most of the exposure of the general population to elevated levels of ammonia is a result of these products.

2.2 Refrigeration facilities

The information in this section is collected from Dincers *Refrigeration systems and applications* [15] unless stated otherwise.

In the words of Rudolf Clausius, the second law of thermodynamics says that "heat can never pass from a colder to a warmer body without some other change, connected therewith, occurring at the same time" [19]. In other words, heat naturally flows from a hotter to a colder body when no interference occurs. In the case of refrigeration systems, the opposite occurs, and heat is removed from a colder environment and added to a warmer environment. For this to happen, work needs to be done on the system to force the heat transfer in the opposite direction.

2.2.1 The vapor-compression refrigeration cycle

A refrigeration facility is typically based on a vapor-compression refrigeration system due to its high coefficient of performance compared to, for instance, the vapor absorption system. In this refrigeration system, the refrigerant changes phase, and absorb and release heat while doing so.

Figure 2.1 shows a simple single-stage vapor compression refrigeration cycle. First, the refrigerant with low temperature and pressure enters the compressor as a saturated vapor where work is done on the gas. In the process of becoming a superheated vapor the gas is heated up as the pressure increases. The pressurized gas proceeds on to the condenser where the gas releases heat and exits as a liquid. The condenser is where the refrigerant releases the excess heat, its latent heat of condensation, and the heat is released to a warm environment. When exiting the condenser, the now saturated liquid proceeds on to the expansion valve. Here, the liquid experiences an abrupt pressure drop, and consequently the liquid expands and immediately boils as evaporation occurs. The liquid absorbs heat due to it being at a lower temperature than the

surroundings and absorbs an amount corresponding to its latent heat of evaporation. The heat absorbed is consumed from the colder environment, which here is the refrigerated area. The refrigerant, now in the gas phase, proceeds back to the compressor and repeats the cycle.

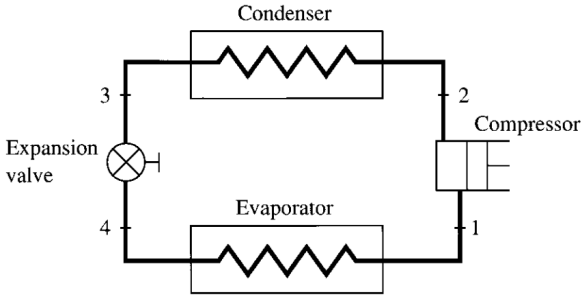

Figure 2.1: A simple single-stage vapor-compression refrigeration cycle showing the stages the refrigerant goes through in this system. Rendered from Wangs *Handbook of air conditioning and refrigeration* [20].

2.3 Dispersion

The information in this section is collected from Mannan's *Lees' Loss Prevention in the Process Industries* [21] unless stated otherwise.

To disperse something is according to Oxford Dictionaries defined as "the action or process of distributing things or people over a wide area" [22]. In the particular situation studied, the substance being distributed is a gaseous substance. The reason for the dispersion can be natural diffusion, external factors such as wind, or a combination of these.

Several different dispersion situations can develop, depending on certain factors. Depending on the release mechanism, three different types of behavior of the fluid flow can be seen. If a pressure drop across the orifice governs the release, it will attain a jet-like behavior [23]. When density irregularities occur due to body forces, the fluid flow is defined as a plume. The third kind is passive dispersion, caused by concentration gradients between two neighboring fluids.

2.3.1 Factors influencing dispersion

Density, elevation and momentum

The gas dispersing may at the time of the release have a positive, neutral or negative density, compared to the surrounding air. When the gas has a positive density compared to air it means that it will be lighter than air, and thereby buoyant, and will rise in the air column. A positive density can be due to low molecular weight or a high temperature of the gas. If on the other hand, the gas has a negative density, it will fall towards ground level and releases of heavy or dense gases tend to have a negative buoyancy. Several factors can explain why a gas is dense, including low temperature or a high molecular weight of the gas compared to that of air.

The size and elevation of the source, whether it is a point, line or area source, and with what kinetic energy the gas is released, will also affect the dispersion situation. The kinetic energy, i.e. the momentum, will especially affect the extent of air entrainment. The more air entrained in the gas, the more diluted the gas will become, and the concentration is lowered. A release with no momentum, a diffuse release, is especially affected by the wind conditions.

Set apart from the factors involving the gas itself or the way it is released, the greatest impacts on the dispersion is the meteorological conditions and the topography.

Meteorology

The meteorological conditions are probably the most unpredictable factors when it comes to dispersion, and these conditions include wind speed and direction, and the stability of the atmosphere. When looking at these conditions the focus is on the lowest part of the atmosphere, closest to the Earth's surface, called the atmospheric boundary layer. Here, wind is the movement of air, and is caused by the Coriolis effect and pressure differences, which causes the wind to flow in the direction of lower pressure.

Wind speed will vary with height and exactly how this wind gradient will vary is determined by the type of terrain and the amount of congestion, as seen in figure 2.2. Congestion leads to turbulence, which reduces the wind speed, and it can be seen that for urban areas the highest wind speed is reached at a higher elevation than for a planar terrain. In very congested areas with high turbulence, elevation will play an important role. For instance, an elevated release point with dispersion of a buoyant gas will experience higher wind speed than a release at ground level and thereby a more efficient dispersion.

The wind direction is defined as the direction which the wind is coming from. The distribution of wind speed and direction for a particular location can be summarized in a wind rose.

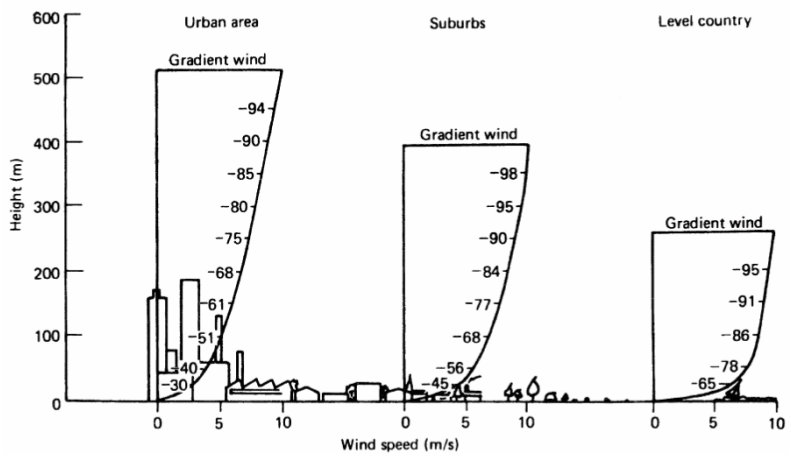

Figure 2.2: Height (m) plotted against wind speed (m/s) showing how the wind gradient differ with varying terrains and amount of congestion. The same wind speed is found at a higher point for urban areas than planar terrains due to turbulence. Collected from Mannan's book *Lees' Loss Prevention in the Process Industries* [21].

The stability of the atmospheric boundary layer can be divided into three categories differentiated by how the air pocket is shifted vertically. This is related to the temperature gradient of the surrounding air, known as the lapse rate. A pocket of air near the Earths surface will be heated up and thereby rise, and how the air pocket will move depends on the temperature gradient of the surrounding fluid. Three categories are defined:

1. Stable: A stable atmosphere is experienced when the rising pocket of air cools quicker than the surrounding air. This leads to the pocket losing its buoyancy and, in the end, falling back to its original location.
2. Unstable: The unstable condition is when the surrounding air cools quicker and the air pocket is always warmer relative to the surroundings. In this way, the pocket maintains its buoyancy and continues rising.
3. Neutral: A neutral atmosphere is met when the pocket cools at the same rate as the surroundings.

A more unstable atmosphere will lead to more turbulence, which leads to more air entrained in the released gas, and quick dilution and spreading can occur. This is why dispersion is normally greatest at unstable conditions, and least at stable conditions.

Pasquill has defined six different classes based on the stability of the atmosphere, varying from very unstable to stable atmospheres. More information about these can be found in Mannan's *Lees' Loss Prevention in the Process Industries* [21].

Topography

Depending on the topography, the dispersion can behave very differently from situation to situation, highly affected by the characteristics.

How the flow is dispersed will, among other things, be influenced by the amount of congestion, the height of the obstacles and the type of surface. The velocity profile, or wind gradient as previously referred to, will vary dramatically over different surfaces. Over a smooth surface, such as ice, the profile will be very different compared to that of, for instance, a wheat field. The variance in the surface roughness and the related wind profile, can be seen in figure 2.2. At an aerodynamic rough surface, a surface where the flow is turbulent at the surface, the roughness length determines the velocity profile. The roughness length depends on the height and the spatial distribution of the objects. If the roughness length, z_0, is not known, it can be approximated by the simple relation where it is related to the mean height of the roughness objects, ε

$$z_0 = \frac{\varepsilon}{30} \tag{2.1}$$

This relation is also provided in the FLACS user manual [24], as a rule of thumb when determining the roughness length, or ground roughness, as it is named in the manual.

2.3.2 Dispersion modelling

Due to the complex nature of dispersion, and all the factors governing the development, dispersion models are often used as a mean to predict how the gas will spread. The model applied in a given scenario is related to the density of the dispersing gas relative to that of air. Several models are available for dispersion modelling, but only two are introduced below.

A model often used for the lighter gases with positive buoyancy is the Gaussian model, which assumes that the dispersion follows a Gaussian distribution. Here, the fundamental equation for diffusion of gas is solved and the dispersion is assigned a given distribution depending on if the source is elevated or not.

A dense gas will portray a very different dispersion behavior. This type of gas has a tendency to sink towards the lowest point possible and spread along the related surface due to its negative buoyancy. For this category of gases, a commonly used model is the box model. The gas cloud is assumed to have a pancake-shaped form, which shows the same properties all through the height of the cloud, and in the crosswind direction.

In addition to different models for gases with different densities, there are also models for dispersion in varying settings, such as dispersion over sea, buildings and terrains of increasing complexity. The common denominator for many of the models is that they are based on assumptions that make them valid only in very simple situations, and thereby not applicable for most situations. A dispersion model not mentioned in Lees' book, which can account for more complex and realistic situations, is the method of computational fluid dynamics (CFD).

2.4 CFD

In many industries, especially in the process industry, one encounters problems where fluids in motion are involved. The objective of CFD is to study the motion of fluids, this including fluids flowing past objects and obstacles. Due to the exponentially increasing computer power, the use of CFD has been made available for the average person. Therefore, the use has increased rapidly in the last decades and will continue to do so in the years to come.

CFD is the art of replacing a set of governing equations with algebraic equations solved at given time steps and spatial locations. These governing equations are all derived by applying a certain physical principle to a certain model of fluid flow, and thereby leads to the governing equations in either partial differential or integral form. The three physical principles that all fluid dynamics are based on are:

1. Mass is conserved.
2. Newton's second law, $\boldsymbol{F} = m\boldsymbol{a}$.
3. Energy is conserved.

2.4.1 Governing equations

This section is highly based on J. D. Andersons book *Computational fluid dynamics - the basics with applications* [25] unless stated otherwise.

Continuity equation

The continuity equation is based on the first physical principle, that mass is conserved. That mass is conserved can be explained as easily as in McCabe, Smith and Harriott's book *Unit operations of Chemical Engineering* [26]:

Rate of mass flow in - *Rate of mass flow out* = *Rate of mass accumulation*

When applied to the model of an infinitesimally small element fixed in space it leads to the continuity equation in *partial differential form*,

$$\frac{\partial \rho}{\partial t} + \nabla \cdot (\rho \mathbf{u}) = 0 \ , \tag{2.2}$$

where ρ, t and $\boldsymbol{u}$ represents density, time and the local velocity vector, respectively. The first term denotes the accumulation, or loss, of mass in the system, and the second term represents the difference between inflow and outflow. The second term involves the *divergence*, a vector operator, defined as

$$\bigtriangledown \equiv \mathbf{i}\frac{\partial}{\partial x} + \mathbf{j}\frac{\partial}{\partial y} + \mathbf{k}\frac{\partial}{\partial z}. \tag{2.3}$$

Momentum equation

The momentum equation is based on Newton's second law, which states that the sum of forces acting on a moving body is equal to the product of its mass and acceleration. The forces acting on the body is a combination of body and surface forces, where the body forces include gravitational,

electric and magnetic forces, and surface forces are present as pressure and shear and normal stress.

By applying the second physical principle to the model of an infinitesimally fluid element moving with the flow we obtain the momentum equation. In the x-direction, we obtain the following relation

$$\rho \frac{Du}{Dt} = -\frac{\partial p}{\partial x} + \frac{\partial \tau_{\mathrm{xx}}}{\partial x} + \frac{\partial \tau_{\mathrm{yx}}}{\partial y} + \frac{\partial \tau_{\mathrm{zx}}}{\partial z} + \rho f_{\mathrm{x}}. \tag{2.4}$$

Corresponding equations is obtained in the y- and z-direction.

Energy equation

The first law of thermodynamics describes the third physical principle: energy is conserved. When applying this to the model of a fluid element moving with the flow, the first law states that

$$\begin{array}{ccccc} \textit{Rate of change of energy} \\ \textit{inside the fluid element} \end{array} = \begin{array}{c} \textit{Net flux of heat} \\ \textit{into the element} \end{array} + \begin{array}{c} \textit{Rate of work done on} \\ \textit{the element due to body} \\ \textit{and surface forces} \end{array}$$

The energy equation has several forms differentiated by terms included or not included in the current situation studied and these are not covered here. More details about the derivation and different forms of the energy equation, in addition to the continuity and the momentum equations, can be found Anderson's book [25].

Concluding the system of equations

For a viscous flow, the above equations combine to what is called the *Navier-Stokes equations*. For an inviscid flow, the term for the equations is the *Euler equations*. Previously, only the momentum equations where referred to as the Navier-Stokes equations, and only the continuity and momentum equations as the Euler equations, but there is now broad acceptance to include the whole set of equations in each term.

The set of governing equations combine to a set of five equations with six unknowns. Hence, to make the system possible to solve, we need to provide an equation for the last unknown. This is done by including the equation of state

$$pM = \rho RT, \tag{2.5}$$

where p is pressure, M is molecular weight, ρ is density, R is the universal gas constant given to be 8.314, and T is temperature. The equation above also brings by temperature as a seventh unknown. Thereby, the last equation needed to close the system, and account for temperature, is a well-known thermodynamic relation, namely $dh = c_p dT$.

2.4.2 Boundary conditions

All problems within CFD are based on the same set of equations. The way to differentiate the scenarios, and make the equations fit the exact problem, is to introduce and make use of different boundary conditions. When the particular fluid flow model is chosen and applied to

the specific physical principle, and the governing equation in the given form is achieved, then the boundary condition will lead the way to the particular solution to the particular problem. Examples include the so-called "no-slip condition" for a viscous flow, where the relative velocity between the fluid and the surface is assumed to be zero. An equivalent boundary condition can be applied to the same surface in respect to the temperature, and states that the temperature of the fluid at the surface is the same as the surface.

2.4.3 Discretization

In general, partial differential equations (PDEs) can be solved either analytically or numerically. The analytical methods provide expressions for the variables continuously throughout the domain and give exact results, while the numerical methods make use of a different approach and provide approximate results. Instead of finding the solution in an infinite number of locations and at all times, the specific domain is divided into a finite number of locations, called grid points, and the solution is found at specific time steps. An illustration can be seen in figure 2.3. The number of grid points is directly related to the accuracy of the results, with a higher number of grid points leading to better accuracy. This is called *discretization*. In this process, the governing equations are replaced by approximate algebraic equations.

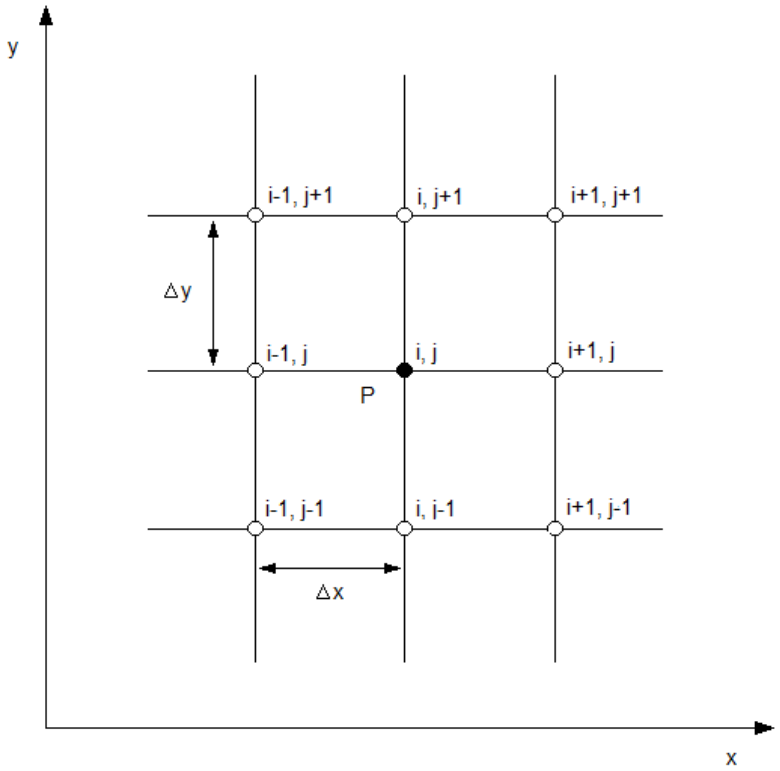

Figure 2.3: An illustration of a structured grid with discrete points in a uniform distribution in the xy-plane. Based on a figure by Anderson [25, p. 126].

There are three discretization techniques widely adopted within CFD; finite difference, finite volume and finite element, where the method of finite differences is the most implemented out of the three.

2.4.4 Turbulence modeling

The information in this section is collected from Warnatz et. al [27] unless stated otherwise.

Turbulence, whether it is in dispersion or combustion, is found as eddies with varying size supplying energy to the flow. A higher amount of kinetic energy is associated with larger eddies, and the energy supply to the flow decreases as the dissipation of the eddies proceed. If it had not been for turbulence, and molecular diffusion was the only contributing factor to the mixing, dispersion would be local and very slow. In order to correctly predict gas dispersion, the energy supplied by turbulence needs to be considered. This can be done by either having a small enough grid to encapsulate the smallest eddies, often in the size of a few millimeters, or turbulence models can be invoked. Different turbulence models exist, where increasing amounts of turbulence is modeled.

Direct numerical simulation (DNS) includes all turbulent eddies, independent of size. This option would be the most desirable if it had not been for the enormous computational time and resulting amount of data.

Another option with a lowered resolution, but yet a more viable option, is the model of large eddy simulations (LES). Here, the Navier-Stokes equations are solved numerically for all eddies above a given size, and below it turbulence models, like the k-ϵ-model, are invoked. The use of these turbulence models are based on the assumption that below a given scale the turbulence can be described by an isotropic model.

The option chosen in FLACS, is the method of Reynolds-averaged Navier-Stokes (RANS) equations. These equations are density-weighted averaged, called *Favre-averaged*. An arbitrary property of the flow is divided into an averaged and a fluctuating component, where the fluctuating component accounts for the turbulence.

2.4.5 FLACS

The information in the following section is collected from the FLACS user manual provided with the software [24].

Gexcon AS, a consultant company owned by Christian Michelsen Research (CMR), holds the full proprietary rights to FLACS. FLACS is a CFD tool designed and widely used for a broad span of process safety applications. The development of the software started in 1980 and the scope has highly broadened. Starting as a tool for examining gas explosions offshore, it has now developed into a tool used both ahead and in retrospect of unwanted incidents such as jet fires, blast and shock wave propagation, and dispersion of toxic, asphyxiating and flammable gas.

FLACS depend on turbulence models based on the RANS-equations such as the k-ϵ model for turbulence closure. The software Favre-averages equations for mass, momentum, enthalpy, turbulent kinetic energy (k), rate of dissipation of turbulent kinetic energy (ϵ), mass fraction of fuel and mixture-fraction. The equations are solved on a Cartesian grid using a finite volume method and the SIMPLE pressure correction scheme is used to solve compressible flows while the SIMPLEC scheme is used for non-compressible flows. FLACS uses the finite volume method to discretize the governing equations. The unique thing about FLACS, separating it from other CFD tools, is its distributed porosity concept. With this, the grid cells are assigned area and volume porosities providing a porosity field representing congestion and confinement.

Dispersion of gases in the atmospheric boundary layer is also based on the same set of equations, where buoyancy effects are accounted for with additional terms in the momentum and turbulence equations. Meteorological conditions, such as wind speed and wind direction, and temperature and the turbulence parameters, k and ϵ, are given specific profiles at the inlet boundaries.

Validation

FLACS has previously been used to model gas dispersion in varying scenarios, and has undergone numerous validations. For the purpose of this study, it is considered an appropriate tool. For more information about some of the validation procedures executed on FLACS, the reader is referred to Hansen et al. [28], Hanna et al. [29] and Hanna et. al [30].

The pool model has only been validated for a handful of scenarios, not including pool formed of ammonia. Thus, this is an attempt to try to make FLACS accept ammonia as an input for pool simulations. Per completion of this thesis, FLACS is still not validated for this purpose.

Chapter 3

Pool simulations

The two next chapters present the procedures undergone when the simulations were set up. The simulations in this thesis were split in two parts, where the first section is pool simulations involving liquid ammonia and corresponding evaporation. The second part is dispersion simulations of ammonia in its gaseous state. This chapter focuses on the pool simulations, while chapter 4 describes the dispersion simulations.

The current chapter describes the grid, and the parameters involved in specifying the gas and determining the pool scenario. The output and results from these simulations is presented at the end of the chapter.

3.1 Case description

The situation studied is a thought-of scenario assumed realistic. The greater part of the details in the scenario is actual facts, like the terrain and surrounding structures in the geometry, while some aspects have been modified to fit the simulations. The pool simulations were performed to get information about the concentration distribution obtained in the room, wanting to use this as input for the dispersion simulations.

The assumed situation is a breach in one of the transitions of a pipe located below a storage container holding 750 kg of ammonia at -31°C and 0.1 bar overpressure. The container is located in a machine room which is in connection with, but not directly located within, a refrigeration facility. As the ammonia leaks and forms a pool on the ground, heat is supplied to the liquid and the toxic substance will evaporate and eventually rise. The liquid evaporating leads to the gas flowing towards the emergency ventilation located in a corner of the room, and to it being ventilated out to the surroundings.

The evaporation rate and the rate of ammonia gas flowing through the ventilation could in theory be calculated. When the liquid forms a pool on the ground its rate of evaporation will depend on its temperature ahead of the release, how well it absorbs heat, as well as the open surface available for the liquid to evaporate through and the velocity of wind flowing past the surface. An example of an equation capable of calculating the evaporation rate is one listed in IIAR's ammonia databook [7], given by the U.S. Environmental Protection Agency, and is valid for a 1 cm deep pool of liquid ammonia:

$$\frac{QR}{A} = \frac{0.0597 u^{0.78} VP}{T_R} \tag{3.1}$$

where QR/A combines to make up the evaporation rate given in lb $\cdot$ min^{-1}ft^{-2}, u is wind speed in miles $\cdot$ hour^{-1}, VP is vapor pressure at the temperature of the liquid in psia and T_R is the absolute temperature of the liquid in degrees Rankine.

Along with the equation, a table is rendered where different evaporation rates are listed in accordance with several wind speeds. An evaluation if this equation and its results could be modified to fit this release scenario. Due to very low wind speeds in the machine room it was found inadequate to describe this scenario and the equation was omitted. Instead, an attempt was made to simulate this.

3.2 Simulation setup

The pool simulations were initiated by using a utility program in FLACS called FLASH. In this utility, the user defines a given set of parameters and the output is different variables concerning the fluid flow, such as the leak rate out of the container and mass fraction of the liquid flashing. Due to the storage temperature of the fluid being so close to its boiling temperature at atmospheric pressure, and the low overpressure in the container, only a very small fraction of the fluid flashes at release. The FLASH utility calculated, based on the pressure and temperature, that a mass fraction of only 0.01 evaporates instantaneously.

A selection of the parameters calculated in the FLASH utility is later used as input in the simulation setup.

3.2.1 Grid

The domain was covered in a uniform grid with a cell size of 0.25 m, resulting in a total of 23250 cells. No stretching, refining or smoothing was done. General recommendations for the grid setup include making sure that larger objects align with the grid lines, and here, this was done by aligning the walls with the grid lines.

3.2.2 Geometry

The geometry representing the machine room was put together using boxes and cylinders. The room itself is added as a box measuring 15x7x3.5 m. Some contents was also added, acting as compressors, containers and other components. The full geometry, along with the grid, is shown in figure 3.1.

The main focus has been on adding larger objects down to a certain size, since these will have the largest impact on the available volume for the gas to disperse in. If these simulations were explosion simulations, the amount of congestion would play an even bigger role, and the full geometry would be imitated in greater detail.

3.2.3 Scenario

The setup of the simulation scenarios were all done in the pre-processor CASD, short for Computer Aided Scenario Design. Using a set of sidebars appearing when the desired scenario type is chosen, the user defines the settings of the simulation. All parameters defined in the sidebars are at default given a certain value, which can be changed to fit the scenario. The chosen scenario type in this first part is 'pool', which makes a given set of sidebars to appear. The next paragraphs describes these exact sidebars and the parameters involved.

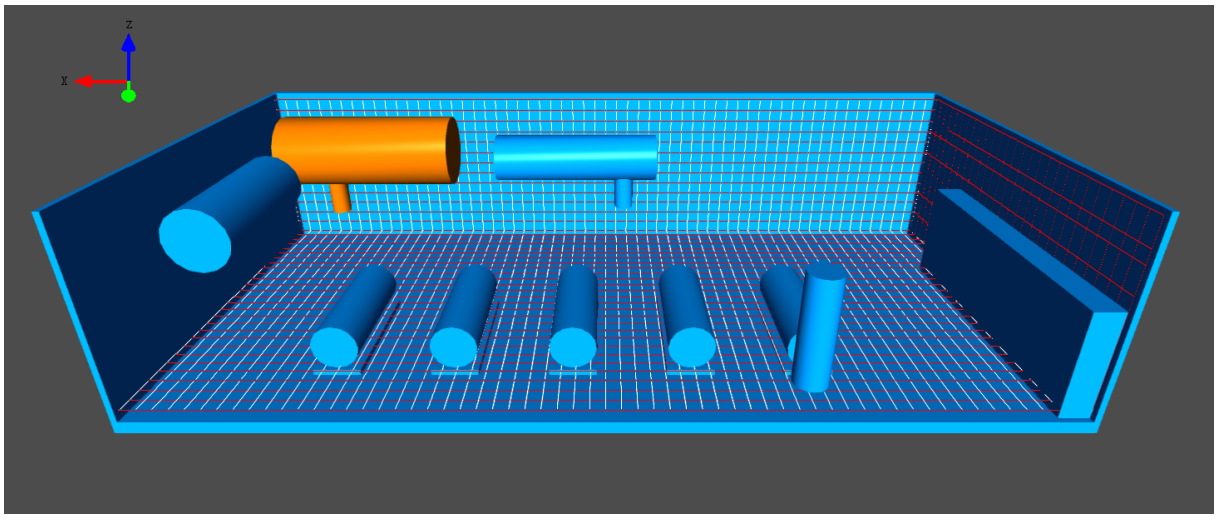

Figure 3.1: A visualization of the geometry for the pool simulations. In the figure, one wall and the ceiling is removed for the purpose of getting a better overview of the room. The grid has been adapted in the figure to make it visible for the viewer. The container colored in orange represents the container where the leak occurs. The red arrow indicates the placement and direction of the inflow of fresh air, while the two blue arrows indicate where air and gas is removed from, acting as emergency ventilation.

Monitor points

Monitor points are spatial locations where chosen values are monitored continuously. Some of the monitor points were added to specific locations, like in front of the suction leaks acting as emergency ventilation, although the greater part was arranged evenly throughout the domain.

The purpose of these first simulations were to try to determine the development of the mass fraction and concentration distributed obtained. Ammonia is not available as a toxic substance, or as a substance at all, in the pool simulations, which make the option of monitoring 'toxic concentration' unavailable as well. Thereby, mass fraction of fuel is the main variable monitored. The full list of monitored variables is:

- Fuel mole fraction
- Pressure
- Temperature
- Velocity vector
- Maximum mole fraction of fuel
- Mass fraction of fuel
- Maximum mass fraction of fuel
- Pool depth
- Pool velocity vector
- Pool temperature
- Velocity of the pool in the x- and y-direction

Single field 3D output

When post-processing the results, several plots can be made, also with variables measured in three dimensions. To do this, the variables have to be monitored in x-, y- and z-direction. The list of single field 3D output correspond to the list of variables monitored at the monitor points. For the full list, see the section above.

Simulation and output control

In this section, variables determining the length of the simulation and how often data is stored in the result file, is set. The only non-default variable is the maximum time set to 300 seconds, where this timespan was chosen to allow the development of a pool and accompanied evaporation to happen.

Boundary conditions

The boundary conditions were all kept at default, 'nozzle'.

Initial conditions

'Initial conditions' is where, among other things, the temperature and pressure of the surroundings are set. The temperature was changed to 20°C, while the rest were kept at default.

Gas composition and volume

As ammonia is not currently an option when choosing the desired fluid in pool simulations, the gas had to be entered manually by defining a set of variables, such as density, molecular weight and critical pressure. The set of variables entered was a set used for test simulations by the owners of FLACS, Gexcon, and the full list of variables and their values can be found in appendix A.

The variables are entered as a user defined species named 'userspec_1'. To get this translated to 'gas composition and volume', the volume fraction of 'userspec_1' is set to '1' to emphasize that the defined species is the sole fluid involved.

Pool

Three pool models exist for the user to choose from; static circular (PM1), dynamic (PM3) and HEM (PM4). The chosen pool type is set to 'dynamic (PM3)', defined in the user manual as "a moving spill where heat and mass transfer is calculated locally in each control volume" [31]. This is in contrast to the static pool (PM1) which, as the name indicate, is a stagnant pool, where macroscopic correlations is used for heat and mass transfer. The third option, HEM (PM4), is chosen for flashing jets involving rain out. Due to the very low mass fraction of ammonia flashing in this situation, it was decided to dismiss PM4 and proceed with PM3.

The pool was placed on the floor with the leak having its origin at x = 12.5, y = 1.5. In figure 3.1 the orange container represents the container where ammonia is leaking from. The formation of the pool is set to start immediately with no initial mass and mass being added to the pool with a rate of 6.52 kg/s, which was calculated through FLASH.

Pool leaks

In the sidebar 'pool leaks', the leak profile of the pool formation can be varied. The leak location is set below the container, with the full hydrostatic column above it. Hence, it is assumed that, as the liquid is leaked and the gas expands in the container, the leak will maintain a relatively constant rate until the container is empty. With the given mass flow rate and specified amount of 750 kg, the container is empty in 115 seconds.

Leaks

To imitate actual conditions, three leaks were added to act as ventilation of air both in and out of the room. The first leak is a larger ventilation grate where fresh air is supplied. The type of leak is 'air', which acts as inflow of air only, and is placed on one of the short walls with the size 0.75x0.75 where it supplies air at a mass flow of 0.5 kg/s. The two last ones, making it a total of three leaks, are two 'suction' leaks, which is a negative point source, removing air and gas at a rate of 1.5 kg/s each. Figure 3.1 shows the location of the leaks according to the rest of the geometry.

Ignition

Time of ignition is set to 9999 seconds as no ignition is desired.

3.3 Results and discussion

As the set of variables used to specify ammonia was originally only used for test simulations, a verification of these was needed to ensure their viability. When verifying these by addressing another source, a selection of the variables proved to be wrong. Specifically, the three enthalpy constants for the gaseous phase, where two of the variables were overestimated and the last was highly underestimated. When applying the new variables, the simulations resulted in no fuel formation, and the program crashed and did not provide any results. Due to time limitations, it was decided to proceed with the dispersion simulations without having the desired input for these, while at the same time trying to solve the error with no fuel formation in the pool simulations.

To understand why no fuel was formed when the new enthalpy constants were implemented, the attention is turned to the thermodynamics of the system. In order for liquid to evaporate, energy needs to be supplied to it. This endothermic reaction thus indicate that the gaseous phase has to have a higher enthalpy then the liquid phase. In FLACS, the enthalpy of a substance is calculated using the formula

$$h = A \cdot T + 0.5B \cdot T^2 - D \tag{3.2}$$

where A, B and D are the three enthalpy constants, whose numerical value vary with the state and temperature of the substance. Figure 3.2 shows enthalpy plotted against temperature for the liquid and gaseous phase, when the new calculated enthalpy constants for the gaseous phase is applied. For calculation of the constants, the reader is referred to appendix B. It is clear from the figure that the relationship between the two phases is not as one would expect. The liquid phase has a much higher enthalpy than the gaseous phase and hence it is physically impossible for gas to emerge, and is why the simulations resulted in no fuel formation.

The notable difference between the set of constants for the test simulations and the new calculated constants was the third enthalpy constant for the gaseous phase, changing from -1103300 J/kg to 3294235 J/kg. Through trial and error the value for this constant where fuel was formed, was determined. For values above 289 565 J/kg no fuel formation took place. For values below this, the simulations developed as expected with fuel forming, both in the liquid and gaseous form. Figure 3.3 visualizes this and shows enthalpy plotted against temperature when the enthalpy of the gas phase is based on the boundary value of 289 565 J/kg. The intercept between the two lines is at 239.75 K, or -33.4°C, the boiling point of ammonia. Above this, the liquid still has a higher enthalpy than the gaseous phase and makes it impossible to evaporate.

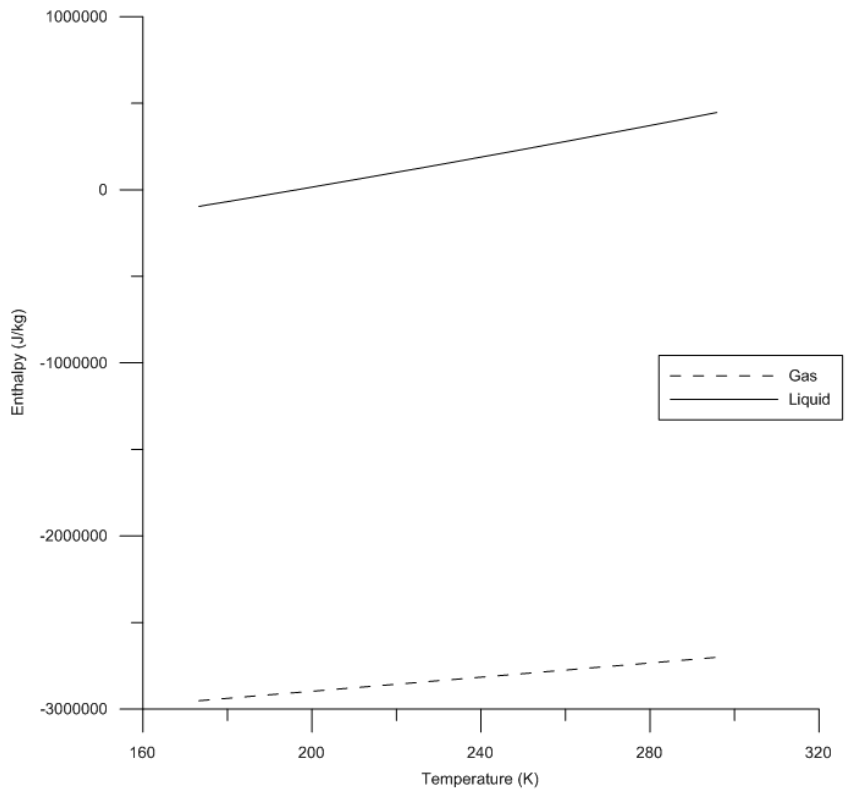

Figure 3.2: Enthalpy (J/kg) plotted against temperature (K) when the calculated enthalpy constants for the gaseous phase is implemented. The liquid phase has a higher enthalpy than the gas, and consequently, no gas can form.

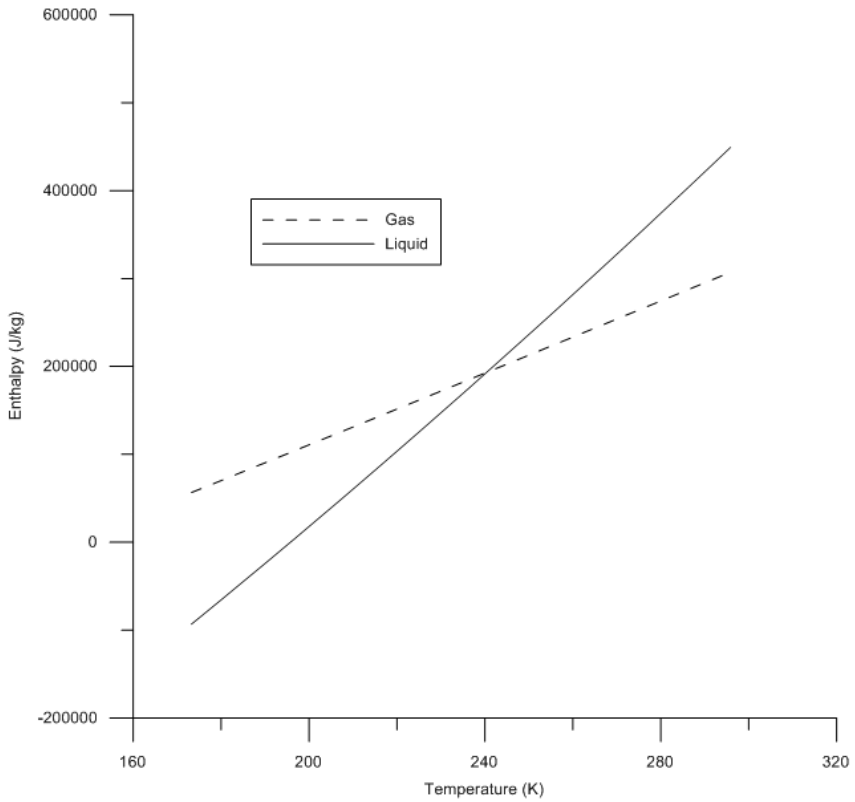

Figure 3.3: Enthalpy (J/kg) plotted against temperature (K) when the boundary value for the third enthalpy constant of the gaseous phase is implemented. Above the intercept between the two lines, at 239.75 K, or -33.4°C, the liquid phase has a higher enthalpy than the gas, and thereby, no liquid can evaporate.

Based on the figures above, the constants for the liquid phase was also examined. The figures clearly show that the relationship between the enthalpy equations for the two phases does not correspond to each other. Thereby, the calculations were made on the constants for the liquid phase as well. The new, proposed values for the two sets of enthalpy constants can be found in appendix B.

As the calculations were completed for the liquid and gaseous enthalpy constants, the resulting relations proved physically possible, as figure 3.4 shows. The new constants resulted in simulations with normal fuel formation. At this point, the simulations involving dispersion was already initiated and no further attention was given the pool simulations.

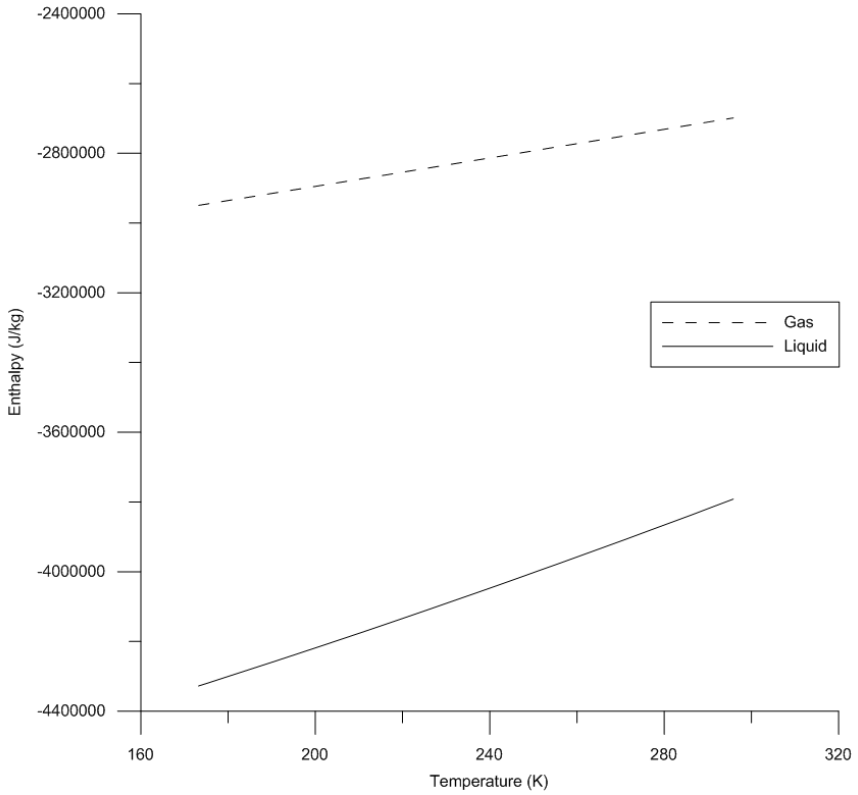

Figure 3.4: Enthalpy (J/kg) plotted against temperature (K) when the new proposed constants for both the gaseous and liquid phase is implemented. The gaseous phase has a higher enthalpy than the liquid phase, and thereby, gas can form.

3.4 Uncertainties

As ammonia is not included in the selection of substances available in the pool simulations, the user itself has to define it. The user can use available variables or calculate them, which introduces human error. Depending on the where the user locates its information, and the starting point of the calculations, the calculated constants can vary greatly.

When calculating the enthalpy constants for the gaseous phase, constants listed in the NIST databook were used. These are listed to be valid in the interval of 298 to 400 K, an interval higher than what would be preferred, as ammonia is not exposed to these kinds of temperatures in this thesis. Still, in the lack of other data they were implemented anyhow.

When determining the heat capacities of the liquid phase, a graph was used and the values had to be read of it. With this, the value read would differ depending on the user and would definitely affect the constants obtained, eventhough probably not greatly.

Chapter 4

Dispersion simulations

This chapter presents the parameters involved in defining the dispersion simulations. The grid, geometry and scenario is described in detail. At the end of the chapter, results and figures describing the results, is presented.

4.1 Simulation setup

4.1.1 Grid analysis

The user manual [24] provides recommendations for grid setup for the different uses of FLACS, and the recommended procedure for dispersion simulations are:

1. Cover the computational domain with a uniform grid.
2. Refine the grid in the near region of the jet perpendicular to the jet axis.
3. Stretch the grid outside the main region of interest towards the boundaries.
4. Smooth from fine grid cells near the jet to normal grid cells further away.
5. For sloping terrains a fine grid is recommended. In this case, 0.2-0.5 m grid cells should generally be used in the z-direction.

Point number two is especially important when it comes to leaks and dispersion, to avoid too much dilution of the jet near the leak source. However, the user manual also states that if the focus of the dispersions is to examine far-field concentrations, than refining around the leak might not be necessary.

Point number one and five is also contradictory. Due to large height differences in the geometry, it was desired to examine the effect a grid can have on the resolution of a sloping terrain by putting both uniform and non-uniform grids to the test.

To determine the best possible grid with the above considerations in mind, a grid analysis was completed. An overview of the different grids studied is listed in table 4.1. As the resulting extent was unknown, and to limit the computational time, only a small area was studied and provided the basis for the grid analysis.

4.1.2 Geometry

The geometry representing the terrain around the facility was imported into FLACS as *.dem*-files. The files is a copy of an industrial area outside Ålesund, Norway, and is an exact replicate of the terrain including height levels. The files were originally much larger, but only the desired

Table 4.1: Overview of the different grids examined in the grid sensitivitiy analysis, with grid size, size of the stretched domain and amount of grid cells.

Grid number	Size of grid, m	Core domain	Size of refined grid, m	Stretched domain	Total number of grid cells
1	1.25	± 10 meter from leak origin in x- and y-direction, ± 5 meter in z-direction	0.251	± 100 meter from leak origin in x- and y-direction, and from 0-60 in z-direction	67 712
2	1.25	± 10 meter from leak origin in x- and y-direction, ± 5 meter in z-direction	-	± 100 meter from leak origin in x- and y-direction, and from 0-60 in z-direction. Max cell size = 2 m	396 576
3	1	± 10 meter from leak origin in x- and y-direction, ± 5 meter in z-direction	0.251	± 100 meter from leak origin in x- and y-direction, and from 0-60 in z-direction. Max cell size = 2 m	597 816
4	x = 0.75 y = 0.75 z = 0.5	± 10 meter from leak origin in x- and y-direction, ± 5 meter in z-direction	-	± 100 meter from leak origin in x- and y-direction, and from 0-60 in z-direction. Max cell size = 2 m	741 321
5	x = 0.75 y = 0.75 z = 0.5	± 10 meter from leak origin in x- and y-direction, ± 5 meter in z-direction	0.251	± 100 meter from leak origin in x- and y-direction, and from 0-60 in z-direction. Max cell size = 2 m	801 837
6	x = 0.5 y = 0.5 z = 0.25	± 10 meter from leak origin in x- and y-direction, ± 5 meter in z-direction	-	± 100 meter from leak origin in x- and y-direction, and from 0-60 in z-direction. Max cell size = 2 m	1 390 212

area of the massive file was snipped and used. This was done to save computational time and to only focus on the relevant area.

An attempt was made to import *.dgn*-files containing buildings and the correct location of these, to ensure full correspondence between size and placement of the objects, but the attempt was unsuccessful due to the acquired files not showing all three dimensions. It was then decided to add parts of the structure manually, starting closest to leak and proceeding outwards.

The purpose of adding the buildings is to include the greatly enhanced vertical mixing which they contribute to. The buildings were added as combinations of boxes and a few cylinders, and rotated around the z-axis and placed in the desired position according to each other. The full geometry is shown in figure 4.1.

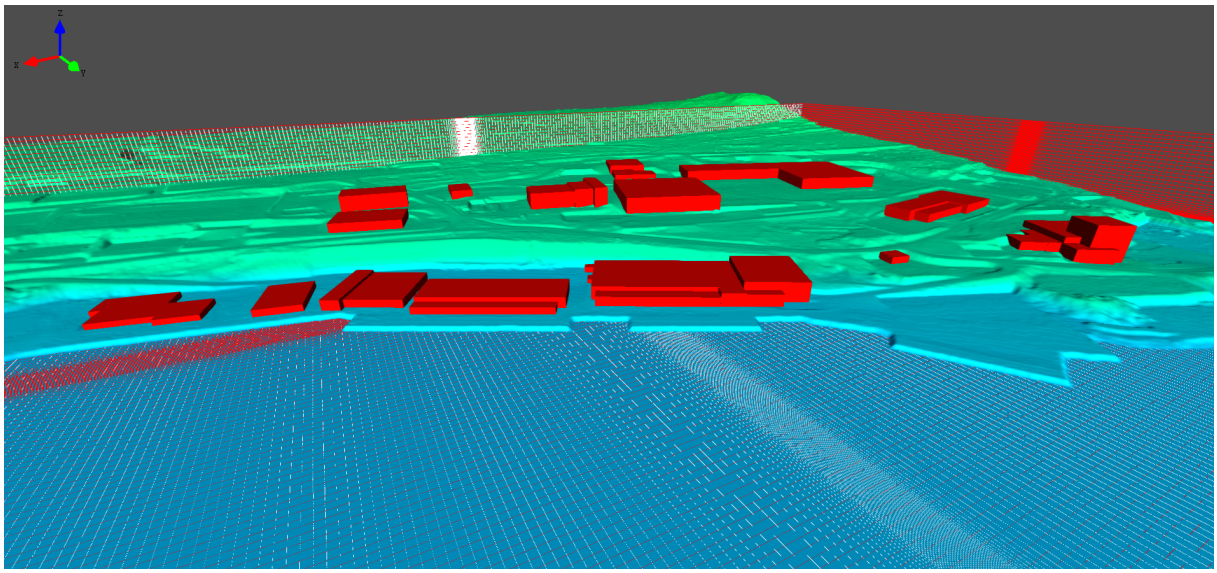

Figure 4.1: A vizualisation of the geometry implemented in the dispersion simulation, with an example of a grid is added.

4.1.3 Scenario

The simulation scenarios were set up in CASD, using the scenario sidebars to define the settings. The chosen simulation type is 'dispersion and ventilation'.

Monitor points

The monitor points were arranged evenly throughout the domain, monitoring the following variables:

- Pressure
- Temperature
- Velocity value
- Velocity vector
- Fuel mass fraction
- Maximum fuel mass fraction
- Toxic concentration
- Toxic dose
- Toxic mole fraction

Single field 3D output

The selected three-dimensional variables monitored is the same as the variables monitored at the grid points, listed above.

Simulation and output control

CFLC and CFLV were the only two changed variables, changing them to 20 and 2, respectively, and keeping them in accordance with recommendations in the user manual. The simulations were run until maximum extent of the dispersion was obtained.

Boundary conditions

When setting up the wind speed and wind direction, the boundary condition 'wind' is automatically chosed at the inflow and parallel boundaries. Nozzle, which is the default, is recommended for the remaining boundaries.

Initial conditions

The outside temperature that the gas is released into was set to 10°C. The user manual provides a table describing the subdivision of the ground roughness levels and was given the value 0.25, according to the description 'high crops, scattered obstacles'. All other variables were kept as the default value.

Gas composition and volume

To specify ammonia as the desired fluid, 'ammonia' is entered in the field of 'toxic specification' and the volume fraction of 'toxic' is set to 1 to emphasize ammonia as the sole gas.

Wind

The wind conditions were given through the 'wind wizard'. Here, the characteristic velocity and the given reference height is set. Different wind speeds and direction have been studied, and combinations of different directions and both high and low wind speeds have been examined. Based on wind data from the actual area, combinations of wind speed and direction have been chosen, and is listed in table 4.2. The data in the table is listed with decreasing frequencies, and the full set of frequencies for the combinations of wind speed and directions is available in appendix C.

Table 4.2: The chosen wind speed and wind directions examined, listed with descending frequency and simulation ID.

ID	Wind direction	Wind speed
100002	150° (S-SE)	2.5 m/s
100012	210° (S-SW)	7.5 m/s
100004	120° (E-SE)	7.5 m/s
100005	180° (S)	2.5 m/s
100015	180° (S)	7.5 m/s
100007	240° (W-SW)	7.5 m/s
100014	150° (S-SE)	7.5 m/s
100016	120° (E-SE)	2.5 m/s
100008	210° (S-SW)	2.5 m/s
100011	270° (W)	7.5 m/s
100013	240° (W-SW)	12.5 m/s
100018	210° (S-SW)	12.5 m/s
100000	60° (E-NE)	7.5 m/s
100017	60° (E-NE)	2.5 m/s
100027	240° (W-SW)	2.5 m/s

4.1.4 Leaks

Leak analysis

Due to the pool simulations not leading to the desired results, the leaks had to be set up based on assumptions and approximations. In order to determine if the way the leak was set up had any impact on the results, a sensitivity study was performed.

A leak analysis was performed on a smaller release of approximately 300 kg. A smaller release was assumed capable of representing the cloud dispersion independent of actual release size. Two simulations with different mass flows and duration were set up to assess the effect of leak rate and leak duration. The first leak setup had a low mass flow and long duration, and the second setup had a high mass flow and shorter duration. Both simulations were run with the same grid and stopped when no fuel was remaining in the domain. The wind characteristics were chosen to a wind coming from E-NE with a speed of 7.5 m/s. The actual mass flows and durations is listed in table 4.3.

Table 4.3: Total mass flow and duration of the two leak setups in the leak analysis.

Leak setup	Total mass flow from the two leaks (kg/s)	Duration (s)
1	0.65	462
2	1.95	154

Leak setup

An equivalent to the 'wind wizard', the 'leak wizard', was used for the setup of the leaks. Here, the position, size and profile of the leak is determined. Two leaks were added acting as the outlet of the emergency ventilation, using the 'jet' type. Based on a circular fan of 20 centimeter, the leaks were given a corresponding area, and ordered to flow in the x- and y-direction, as seen in figure 4.2. The leaks were set up with a leak rate corresponding to the maximum mass flow of the actual emergency ventilation located at the facility, listed to be 1.5 kg/s, making the total leak rate of ammonia 3.0 kg/s. The leaks were set to run until the total amount of 750 kg had flowed through the ventilation. Knowing that what actually comes out of the ventilation would realistically be a mixture of both ammonia and air with a varying mixture ratio, this is not fully correct.

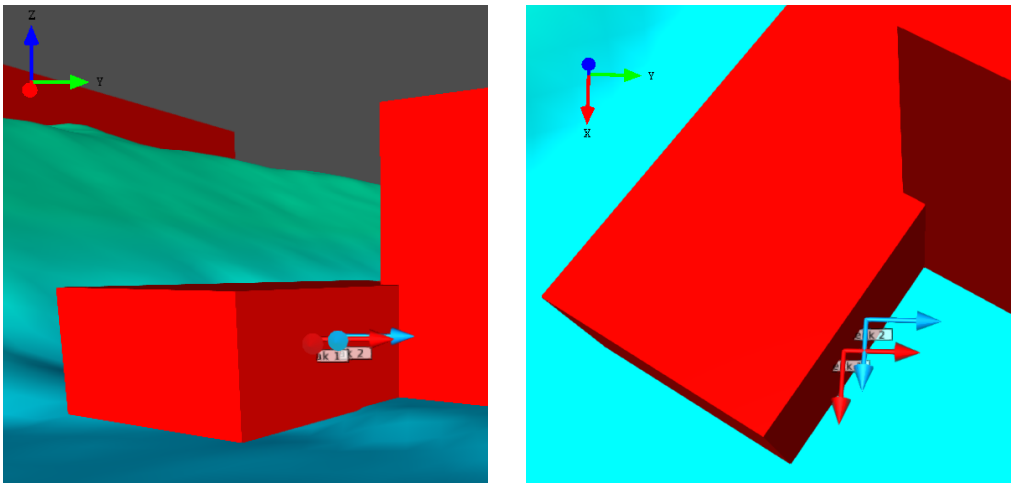

(a) **(b)**

Figure 4.2: The two leaks seen from (a) NE and (b) above.

4.2 Results and discussion

The figures in this section is plotted with various concentrations, where most of the threshold concentrations is rendered from section 2.1.2. The conversion factor from ppm to mg/m^3, which FLACS reports the concentrations in, is approximately 0.7.

1. 100 mg/m^3; half of 'IDHL' of 300 ppm
2. 200 mg/m^3; 'IDHL' of 300 ppm
3. 700 mg/m^3
4. 1750 mg/m^3; the lower limit of 'dangerous to life' at an exposure of 30 to 60 min
5. 3500 mg/m^3; the lower limit for 'fatality' at an exposure of 30 to 60 min
6. 7000 mg/m^3

4.2.1 Grid analysis

A grid analysis was conducted on a scenario where ammonia was leaking for 150 seconds with a total mass flow of 3.0 kg/s from the two leaks combined, resulting in a release of 450 kg. The wind came in from E-NE with a speed of 7 m/s. The simulations were run for a total of 200 seconds, which was decided an adequate time span for the development of the gas cloud. The purpose of the analysis was to determine a grid size that provides a high enough resolution of the domain, with an acceptable amount of computational time.

Of the six total simulations, two yielded the error message 'mass residual', indicating that there was a problem reaching a converged solution. In dispersion calculations, a handful of circumstances can lead to this error. The first, coarsest grid did not have a maximum cell size set, and according to the user manual, a big difference between the smallest and largest grid cells can cause this error. The span of cell size stretched from 0.251 m in the refined area, to 8.4 m by the boundaries, and thereby probably leading to the described error.

The second grid reporting the error message is the finest grid, grid number 6, where the error occurs right after the leak has stopped. When this error occurs right after the leak stops, it can

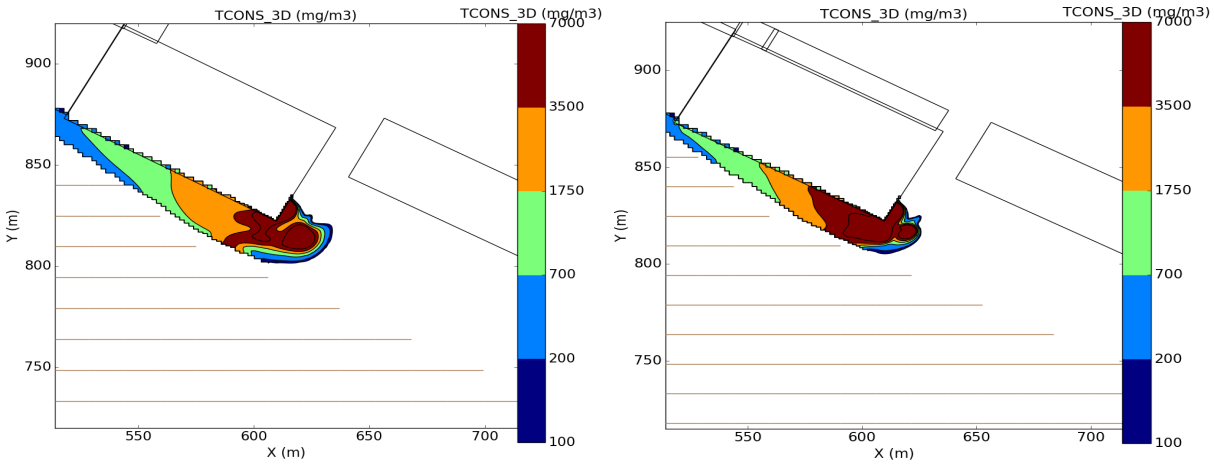

Figure 4.3: Two-dimensional cuts in the xy-plane of ammonia dispersion with a concentration larger than 100 mg/m^3 at z = 9.75 m and t = 70 seconds for (a) grid number 4 and (b) grid number 5. The two grids have the same grid dimensions of 0.75 m in the x- and y-direction, and 0.5 m in the z-direction, but (b) has been refined around the leak.

easily be fixed by modifying the leak profile. However, due to extensive computational time it was decided to not proceed with this grid size.

When the coarsest and finest grid is excluded, four grids are left with grid sizes ranging from 1.25 to 0.5 m. When studying the dispersion in FlowWis it appears that grid number 2 estimates a larger exposed area than the other three. When the concentration of ammonia is calculated in the domain, the average concentration in the whole grid cell is reported. Thereby, a grid with larger grid cells will average over a larger area. The overestimation appears to decrease with grid sizes of 1 cm or less, and grid number 2 is thus dismissed.

Another phenomenon observed in the post-processing, is the leaking of gas through walls and larger objects. The user manual describes this effect as something that can happen when larger objects are not aligned with the grid lines. In this thesis, the structures surrounding the facility is a replica of an actual area, and it was decided that aligning the buildings would create an unsatisfying copy and no aligning was performed. With that in mind, leaking was expected, and did appear. As the leaking decrease with decreasing grid size, and is greatly lowered in grid number 4 and 5, grid number 3 is also dismissed.

The object of this thesis is to capture far-field concentrations and the user manual suggests that refinement around a might not be necessary, and can be skipped to save computational time. The two remaining grids, grid number 4 and 5, differ only in the refinement around the leak, and was chosen specifically to study the effect of refinement.

Figure 4.3 shows that as the dispersion progresses, they both portray the same behavior with little differences. The refined grid results in a better gradient near the leak, but the concentrations achieved at the near vicinity of the release point would still be fatal to the ones exposed, with or without a refined grid.

However, when looking at selected monitor points, differences in the development of the concentration is obvious, as seen in figure 4.4. Monitor points report the concentration in the entire cell it is located within, and as mentioned earlier, this is the average concentration in the whole cell. Some of the monitor points in the refined grid, especially the ones with higher z-values, show a lower concentration than the same monitor point in the non-refined grid. This is due to that, when refinement is done, smoothing happens as well. The smoothing leads to a higher number of cells and better resolution in the z-direction.

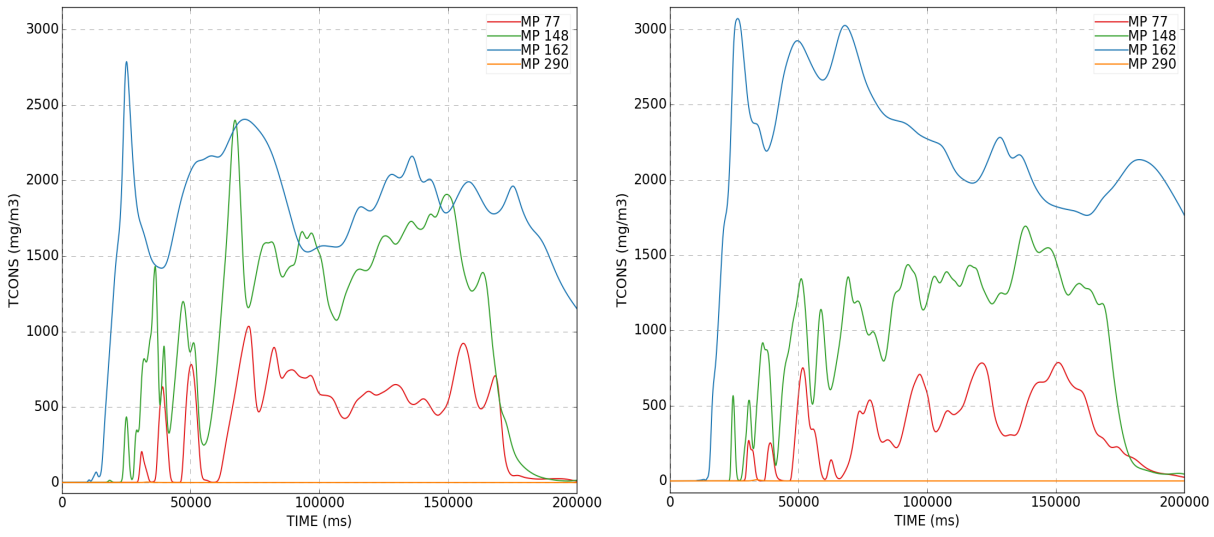

Figure 4.4: Concentration at four different monitor points for (a) grid number 4 and (b) grid number 5.

As an example, monitor point 148 in figure 4.4 have a z-value of 26. In the refine grid, where more grid cells are provided in the z-direction, the monitor point reports a lower concentration than for the same monitor point in the non-refined grid.

Summarized, it appears that the overall extent of the gas cloud is independent of grid refinement, while the resolution in the z-direction is slightly improved with refinement. A good resolution in the z-direction is desired, but as the refinement greatly enhances the amount of cells and computational time, and the main focus is the far-field concentrations, it was decided to proceed with the non-refined grid.

Even though a preferred grid size was determined, the stretched boundaries had to be adjusted according to the wind direction and wind speed, due to the dispersion depending heavily on these. Differing only in the degree of stretching, the cell size was kept at the determined size of 0.75 m in x- and y-direction, and 0.5 in z-direction.

4.2.2 Leak analysis

The results of the leak analysis is visualized in figure 4.5, where the column on the left shows the long duration leak with a low mass flow, and the column on the right shows the short duration leak with a high mass flow.

The post-processing showed that a higher mass flow leads to more of the toxic substance being released in a shorter amount of time, and the dispersion thereby develops quicker. However, the low mass flow leak quickly catches up and attains the same shape and degree of dispersion. In addition to spreading the quickest, the high mass flow leak also dilutes the quickest and disappears.

As the leaks continue they both attain the same shape and no prominent difference in the extent of the cloud is found. What is seen is that the higher flow rate reaches its maximum dispersion quicker and also maintains this extent of dispersion for a longer period. However, almost the exact same extent is achieved. Figure 4.5 shows the dispersion of the cloud with concentration above 100 mg/m^3 at different heights, and it is obvious that the achieved dispersion and shape of the dispersion very much correspond between the two setups.

It is concluded that, for the current setup of the geometry and scenario, the way the leak is defined does not have particular impact on the cloud dispersion achieved.

4.2.3 Extent of the dispersion

In this subsection, selected results are presented. For a complete overview of the results, the reader is referred to appendix D.

When starting the post-processing, some of the simulations showed such an extensive dispersion that the studied domain had to be adjusted and enlarged. The adjusting in some simulations lead to three, almost four, times the amount of cells, and therefore, the grid size also had to be adjusted to maintain an acceptable computational time. For the mentioned simulations, the grid cell size was adjusted to 1.25 in the x- and y-direction and 1 m in the z-direction, with a maximum cell size of 4 meter. This specific combination of grid cells was originally not examined in the grid analysis, but a uniform grid of 1.25 m cells was examined, and it was concluded that this size probably leads to an overestimation of the extent.

Simulations where the extent exceeded the chosen domain, but where the gas clearly extends over sea, no re-run of the simulation was completed.

Further, the error 'mass residual' was encountered at this stage also, resulting in sudden crashes for some scenarios. For the mentioned instances, when problems of reaching a converged

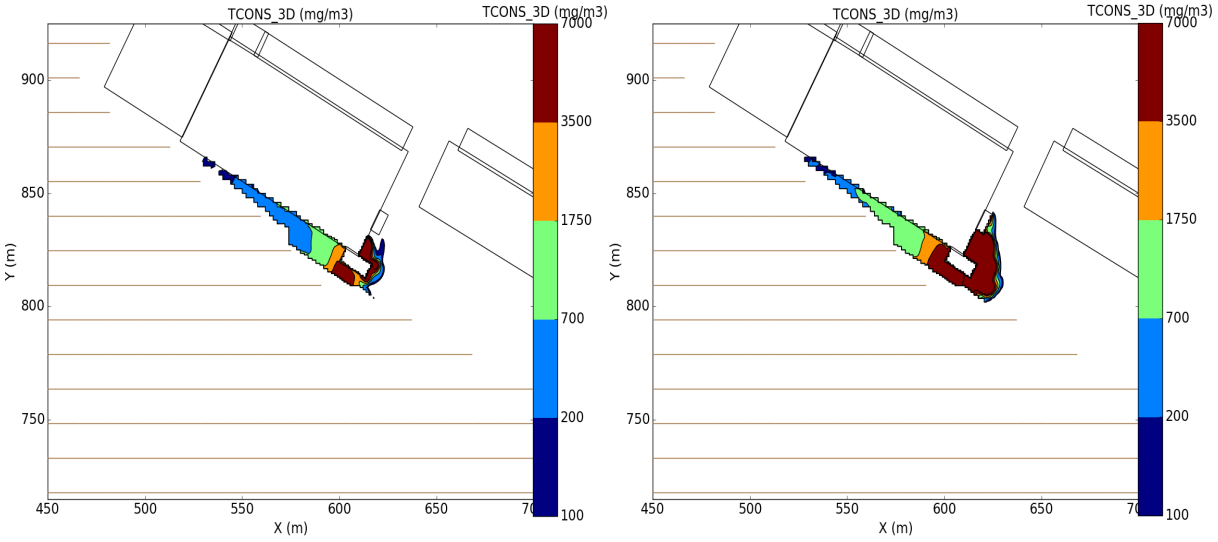

(a)

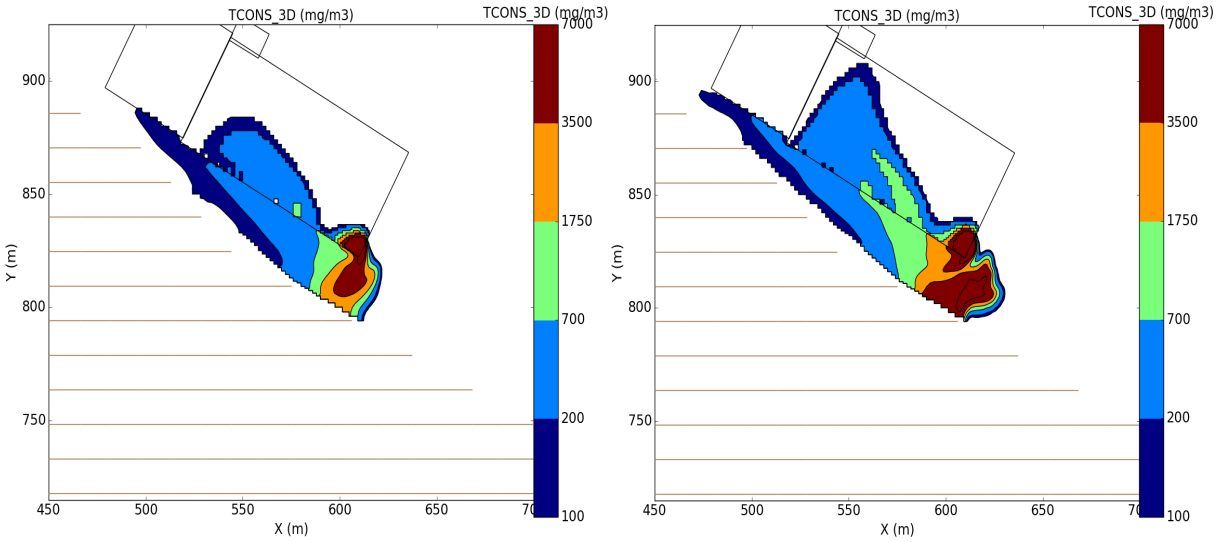

(b)

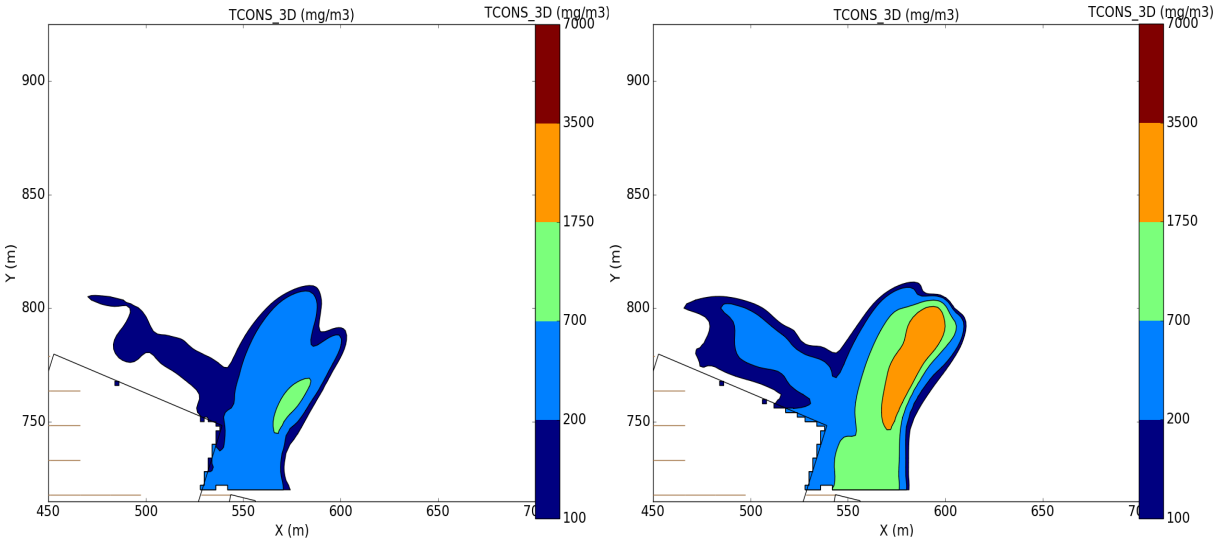

(c)

Figure 4.5: Two-dimensional cuts in the xy-plane of the toxic gas cloud with a concentration above 100 mg/m^3 from a simulation of a leak with a low mass flow and long duration on the left, and a leak with a high mass flow and short duration on the right, at (a) z = 3.75 m, (b) = 12.2 m and (c) = 25 m.

solution occur, recommendations in the user manual was ensued. Here, the user is advised to reduce CFLC and CFLV by a factor of 2, reducing them from 20 and 2, to 10 and 1, respectively.

Table 4.4: Maximum extent on land with concentrations larger than 100 mg/m^3 for the combinations of wind directions and wind speeds, sorted with descending frequency. The extent is calculated using the Pythagorean theorem.

ID	Wind direction	Wind speed	Extent over land
100002	150° (S-SE)	2.5 m/s	629 m
100012	210° (S-SW)	7.5 m/s	127 m
100004	120° (E-SE)	7.5 m/s	731 m
100005	180° (S)	2.5 m/s	217 m
100015	180° (S)	7.5 m/s	164 m
100007	240° (W-SW)	7.5 m/s	185 m
100014	150° (S-SE)	7.5 m/s	331 m
100016	120° (E-SE)	2.5 m/s	718 m
100008	210° (S-SW)	2.5 m/s	157 m
100011	270° (W)	7.5 m/s	1424 m
100013	240° (W-SW)	12.5 m/s	193 m
100018	210° (S-SW)	12.5 m/s	72 m
100000	60° (E-NE)	7.5 m/s	778 m
100017	60° (E-NE)	2.5 m/s	181 m
100027	240° (W-SW)	2.5 m/s	1660 m

When the problems were solved, and the simulations were completed, the results could be processed. As a way of categorizing the results, the extent over land of the gas cloud where the concentrations exceeded 100 mg/m^3, was calculated for each scenario using the Pythagorean theorem. Table 4.4 lists the simulations with the same decreasing frequency as previously shown, and with the corresponding extent. According to table above it appears that the set of simulations can, with one exception, be split into two categories:

1. Dispersion in the near proximity of the leak, with an extent of less than, or approximately, 200 meter.
2. Dispersion to more distant areas, with an extent greater than 600 meter.

The first category consists mostly of winds coming from the southern directions, in the interval of S to W-SW, with one exception in simulation 100017. Representing the first category, figure 4.6 shows simulation 100013, which displays the highest concentrations furthest away from the leak, and the second longest dispersion, in category 1. This category of simulations prove to disperse in the same, short-range area affecting the nearby buildings just right of the facility and for some, the two located directly behind uphill. With the wind in this category mostly being supplied from the southern directions, the largest portion of gas is dispersed out to sea. However, a fraction of the gas is dispersed upwind, where it covers and blurs a nearby road, as well as objects located here. The reason for this unexpected dispersion path is turbulence created at and around the release due to the placement of nearby buildings, forcing the dispersion in directions that originally were not expected. When dispersing up the hill, the gas is eventually slowed down and stopped by the structures here, supplying a concentration of up to 1750 mg/m^3.

Figure 4.7 show the field of velocity vectors in the yz-plane close to the leak. With the wind coming from the left, one can clearly see the eddy formed in lower center part of the figure, where

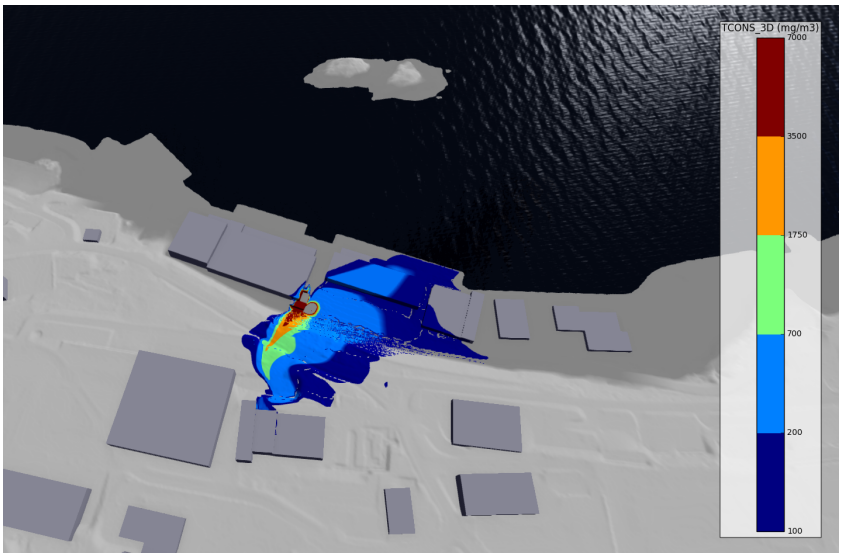

Figure 4.6: Three-dimensional surface plot showing dispersion of ammonia gas with concentrations greater 100 mg/m^3 when the wind enters from W-SW with a wind speed of 12.5 m/s, 230 seconds into the release.

the velocity is in the opposite direction of the wind direction, and driving the gas towards, and up, the hill. In general, this effect is seen for most of the wind directions in the interval of E-SE to W-SW, where 11 out of the 12 most frequent combinations are located. This turbulent effect is also seen parallel to the hill, leading to a wider dispersion normal to the wind direction.

For the second category of simulations, where the dispersion extends more than 600 meters, mostly areas along the shore is affected. With four out of six dispersing along the shore, in either direction, this group might not be considered that dangerous as certain other wind directions where the dispersion is inwards on land, even though their extensive dispersion alone might indicate so.

Figure 4.8 show one of six simulations in this category. With the wind entering at E-SE and 7.5 m/s, the wind does not have path parallel to the terrain and the wind forces the gas up and over the hill to the left of the facility, affecting a wider area than several of the others in this category. Wind few obstacles in place to change the direction or stop the gas, the dispersion

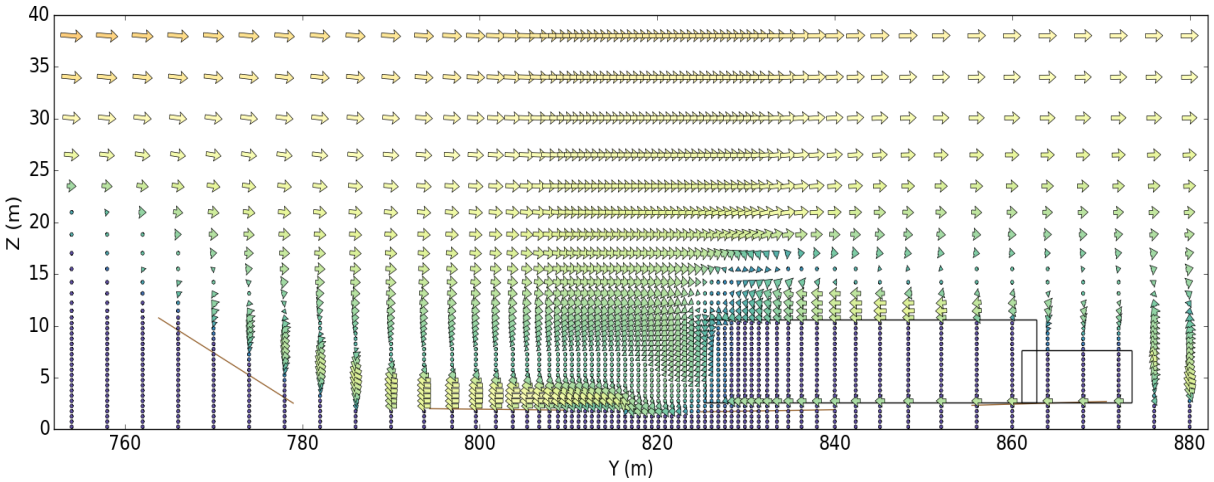

Figure 4.7: Two-dimensional cut in the yz-plane showing the field of velocity vectors close to the leak, with the wind is coming from the left in the figure. In the lower, center part, the turbulent eddy forcing the gas upwind is shown.

continues out to sea. The same behavior is seen for a lowered wind speed 2.5 m/s with the same direction, manifesting that, for this direction, the extent is independent of wind speed as the dispersion continues out to sea.

Obviously, the assumed worst-case scenario is found in category 2. Depending on the criteria, whether it is extent, concentration obtained, affected area or longevity of the cloud, several worst-case scenarios can be defined. Here, it is chosen to present the scenario which probably would cause the most difficult evacuation, as the dispersion is in on land, as opposed to dispersion along the shore only. Figure 4.9 show the dispersion when the wind enters from E-NE with a speed of 7.5 m/s. While it does not bring with it very high concentrations, apart from close to the leak, the relatively high wind speed immediately brings the gas downwind to areas where crowds of people may reside, and concentrations of up to 700 mg/m^3 is encountered for a long period.

As figure 4.9 indicates, the wind directions in the interval of W to E, seems to induce a more extensive, and problematic, dispersion in towards land. It was expected that these directions would present the actual worst-case scenarios, but as they represent combinations with an eminently low frequency, these were originally not studied. To obtain a slightly better sense about how more of the wind directions in this interval would disperse, a dispersion scenario with a wind from N-NW at 2.5 m/s was simulated.

Due to time limitations the simulation was completed with larger grid cells of 2 meter in the x- and y-direction, 1.75 in the z-direction and with a maximum cell size of 6 meter. Due to this, it cannot be directly compared to the rest in this thesis, but is still shown and described here. However, figure 4.10 clearly shows the expected comprehensive dispersion in on land, although the concentrations are relatively low, maintaining a concentration of up to 700 mg/m^3 throughout the cloud. The cloud even dispersed all the way to the boundaries, and probably would have dispersed further if the boundaries were shifted outwards.

The comprehensive dispersion in figure 4.10 might be expected due to the wind direction and the low wind speed, as low wind speeds are not able to heavily contribute to dilution of the cloud. A higher wind speed is expected to disable the buoyant tendency of ammonia gas cloud, forcing it downwards, but also greatly enhance the dilution of it [3].

For many of the wind direction, where both low and high wind speeds are examined, the effect where a higher wind speed dilutes the cloud quicker, is seen and can be observed in table 4.4 initiating this section. When increasing the wind speed from 2.5 m/s to 7.5 m/s at S-SE, the extent is halved. Other affirmative examples include the direction of S-SW, which has three wind speeds studied. For this direction also, an increasing wind speeds leads to a lowered extent. The wind direction shows a dispersion pattern similar to the one in figure 4.6, and the variation in extent is seen in how far the gas is forced up the hill due to the turbulent eddies created. Even though a higher wind speed would be assumed to produce a lot of turbulence, and forcing even more gas up the hill, it appears that the gas is forced out to sea instead, where it is diluted.

On the other hand, the opposite effect is also observed. Even though the difference is small, for both E-SE and W-SW, the higher wind speed disperses the gas further.

When summing-up the most frequent combinations, considerable differences is seen in the extent. The wind directions of the top five combinations, which account for almost 50% of the winds, are located within an interval of only 60°, varying from S-SE to S-SW. However, the extent of the worst out of the five, is almost six times as great as the least prominent.

Therefore, the expected winds provide a wide range of dispersion behaviors. With the location of the facility, with the sea north of it and the wind mostly coming from the southern directions, extensive dispersion is rarely seen. As for Greulich and Hansen [3], the results when it comes to wind directions are more prominent than those for the wind speeds alone.

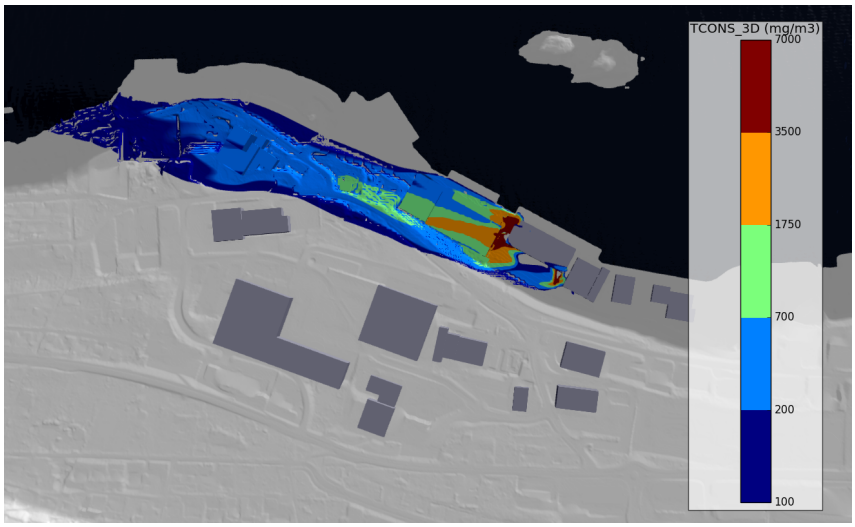

Figure 4.8: Three-dimensional surface plot showing dispersion of ammonia gas with concentrations greater 100 mg/m^3 when the wind enters from E-SE with a wind speed of 7.5 m/s.

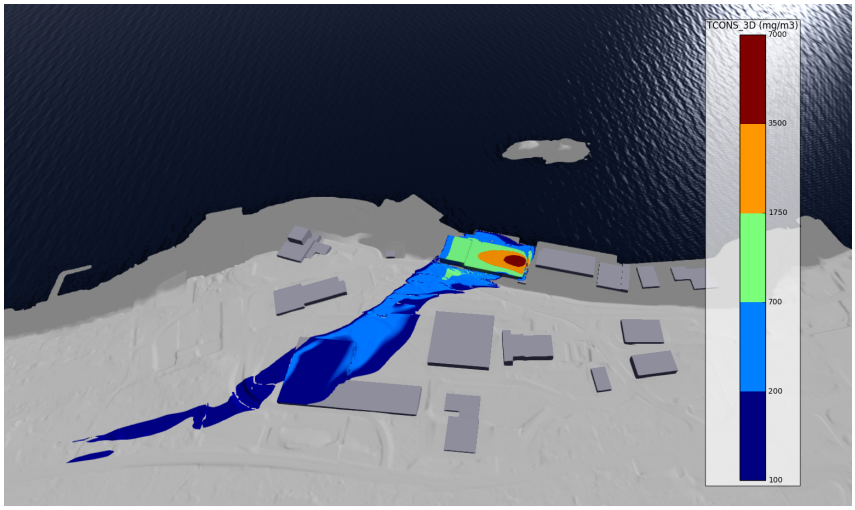

Figure 4.9: Three-dimensional surface plot showing dispersion of ammonia gas with concentrations greater 100 mg/m^3 when the wind enters from E-NE with a wind speed of 7.5 m/s.

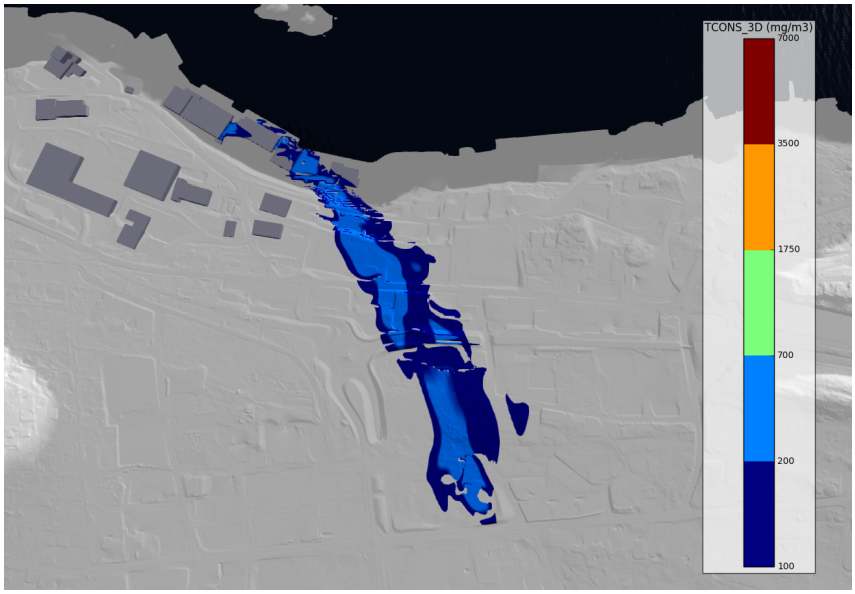

Figure 4.10: Three-dimensional surface plot showing dispersion of ammonia gas with concentrations greater 100 mg/m^3 when the wind enters from N-NW with a wind speed of 2.5 m/s.

4.2.4 The effect of varying parameters

Pasquill classes

In FLACS, the decision of which Pasquill class to apply to the studied atmosphere is based on the weather conditions along with the wind speed [31]. In this thesis, no assumptions were made on weather conditions other than temperature, and the simulations were limited to only focus on the wind speed and direction, and thereby no class was set. Nonetheless, it was still desired to examine the possible effect if any class was actually chosen.

The user manual provides a table where wind speed and weather condition combine and is classified into one of the six Pasquill classes, varying from A to F, from very unstable to stable, helping the user choose the correct class. At the same time, the user manual does not recommend the use of class A to C, due to the instability they can give rise to.

As a basis for comparison, simulation 100005, with a wind from S with a speed of 2.5 m/s, was run with classes D, E and F, which are neutral, slightly stable and stable, respectively. Class A to C was not chosen, as per the recommendations in the user manual. As choosing a Pasquill class is a way of categorizing the amount of turbulence, when a class is chosen, the turbulence parameters are set by FLACS. In contrary, when no class is chosen, the user defines the turbulent parameters itself. In this thesis, when no class was set, all the turbulent variables, such as turbulent length scale and relative turbulence intensity, were kept at default as set when choosing the scenario 'dispersion and ventilation'.

When comparing the three Pasquill classes with the original simulation, the progression of the four simulations differ slightly. The first inequality is the shape of the gas cloud, visualized in figure 4.11, where no class is shown next to class E. In general, running with the three Pasquill classes provide a more complete gas cloud at all z-levels, whereas running with no class show a more fluctuating cloud with fingering tendencies. The fluctuating tendencies cause dispersion in the directions normal to the wind direction and indicates that the combination of wind speed and direction in the original simulation join to form a more unstable scenario then the other three. This instability escalates the vertical mixing. As well as the x- and y-directions, the fluctuations are also observed in the z-direction, where they force the gas upwards and raise the concentration in this direction.

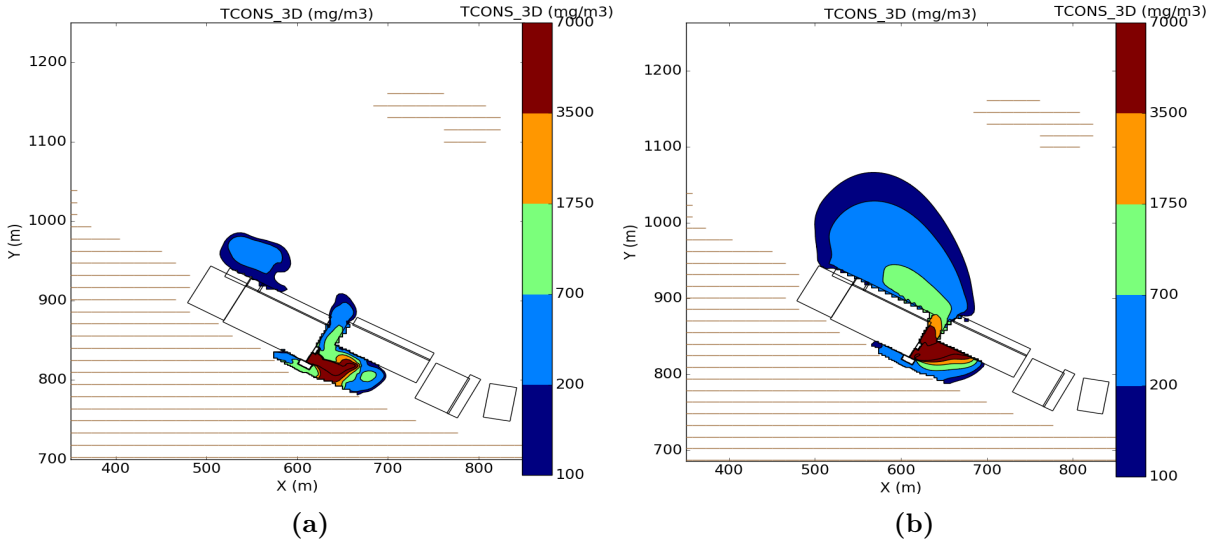

Figure 4.11: Two-dimensional cuts in the xy-plane showing dispersion of ammonia gas with concentrations greater than 100 mg/m^3, for two of four simulations run to examine the effect of implementing Pasquill classes, where (a) is without class and (b) is with class E. The wind enters from S with a wind speed of 2.5 m/s.

Second, when a class is chosen, the wind appears to grab a hold of the gas quicker, and consequently, it is also dispersed and diluted quicker in all directions. However, the gas cloud of the example with no class quickly catches up and attains the same extent. Class D and E very much mimic each other, showing almost identical dispersion patterns, while class F differ slightly and share some of the trademarks of the original simulation. One of the trades shared is that they both show the highest concentrations far above the leak, while it is lowered in class E, and even lower in class D.

Overall, the differences in extent is not remarkable, in any direction. The shape and movement of the cloud differ somewhat, while concentration distributions remain more or less the same. The overall vertical mixing increases without a class and with the large height differences in the studied terrain, adding a class might have induced an underestimation in important areas.

Lastly, as ten of the fifteen scenarios studied have a wind speed located in the interval 0.1-5.2 m/s (see figure C.2 in appendix C), the mentioned table in the user manual lists that these wind speeds can attain all the six classes. A-C was not desired to invoke, and implementing D-F where these were applicable and no class where A-C was applicable, was not considered an appropriate approach. Therefore, the use of all six classes was excluded in this thesis.

Unobstructed dispersion

Knowing that buildings, and obstacles in general, greatly contribute to, and enhance, the mixing of the gas, an unobstructed dispersion was compared with its corresponding obstructed scenario. This was done to attain better into how the obstructions nearby the leak affect the dispersion.

Figure 4.12 display the difference in extent at z = 4.5, slightly lower than the leak, 40 seconds into the release, when the wind enters from W-NW. When no buildings are present, the gas is immediately dispersed downwind as no obstacles is available to suppress it. With a relatively low wind speed of 2.5 m/s, the cloud deviates from the downwind path with a slight upwards movement. The shift is probably due to the direction of the leaks given in the leak setup, as these are set to the x- and y-direction, driving the cloud in the y-direction.

Whereas, with buildings present, obstacles are located directly in line of sight of the leak

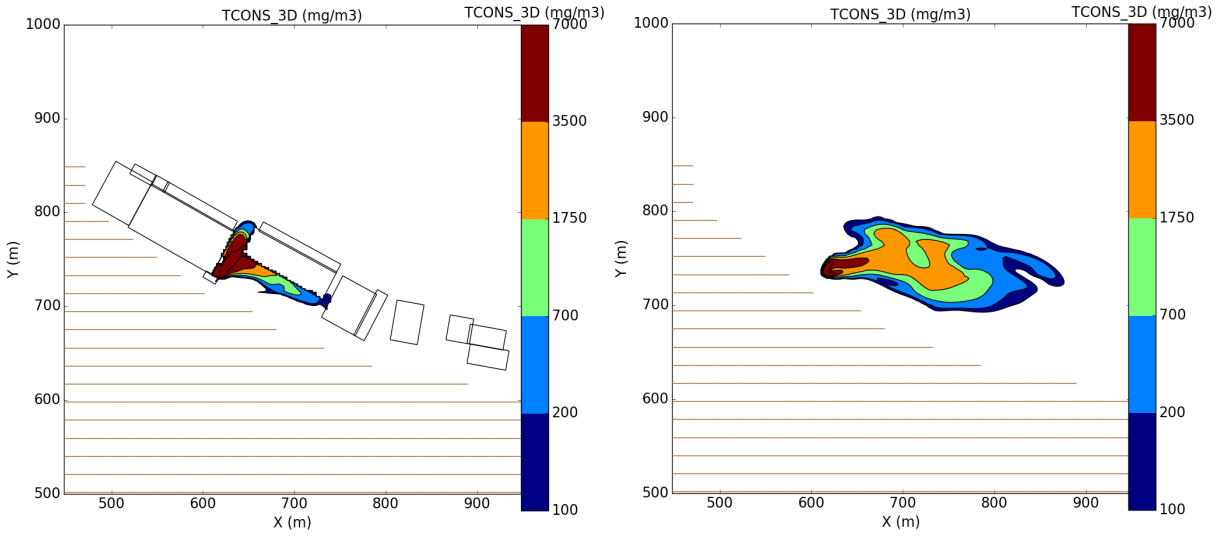

Figure 4.12: Two-dimensional cuts in the xy-plane showing dispersion of ammonia gas with concentrations greater than 100 mg/m^3, at z = 4.5 for (a) an obstructed and (b) an unobstructed geometry, 40 seconds into the release. The wind enters from W-NW with a wind speed of 2.5 m/s.

and form a pocket where gas is stranded. However, when the wind is able to release the large portion of gas located here, it swiftly catches up to the unobstructed dispersion. The mentioned pocket also attains the gas for a longer period, resulting in a lengthy dilution time. Due to the positioning of the buildings, the gas is forced into an elongated cloud, which is in contrast to the more uniformly dispersed cloud when no obstacles are present.

Overall, the leak direction, wind direction and the buildings located in the near vicinity of the leak, all combine and create turbulence. This makes the gas dispersion slower at first, it stays longer in the domain, and spreads more normal to the wind direction. As expected, the generated vertical mixing also leads to higher concentrations further above the leak.

Elevation of the leak

The way the facility is set up, liquid ammonia flows through pipelines on the outside of the building. If a leak occurred here, the release would be a combination of liquid and gas, and would very much compare to the scenario setup in the pool simulations. However, as it does not appear that FLACS is mature enough for a scenario like this, a simplified assumption was implemented. The two leaks were combined to one and moved to a higher z-coordinate, more specifically to the roof of the facility. It was assumed that the same amount of ammonia leaked out through this release also, with a mass flow of 3.0 kg/s releasing in the z-direction. The likelihood of this to happen at this location is probably very low, but it is assumed as a simplification, and is completed to get a sense of the dispersion would progress if a leak occurred here.

As the release point is elevated above any obstacles nearby, no further turbulence is added to the wind field and the wind instantly grabs the gas and drives it downwind. With a low wind speed of 2.5 m/s, the buoyant tendency of the warm ammonia gas is not overcome by the wind and is clearly displayed, as figure 4.13 show a rising gas plume. With no taller buildings or obstacles present up- or downwind of the release, no extra turbulence is created and the gas clearly follows the path outlined by the wind. The wind grabs a hold of the gas immediately, and quickly dilutes it, as the figure displays. As the leak is releasing in the z-direction, the leak is forced even more upwards. This increases the elevation further above the roof and makes it easier for the wind to dilute it.

It appears that, with the conditions explained above, a release here is less extensive and hazardous, as a release closer to ground level, where obstacles creating turbulence is present.

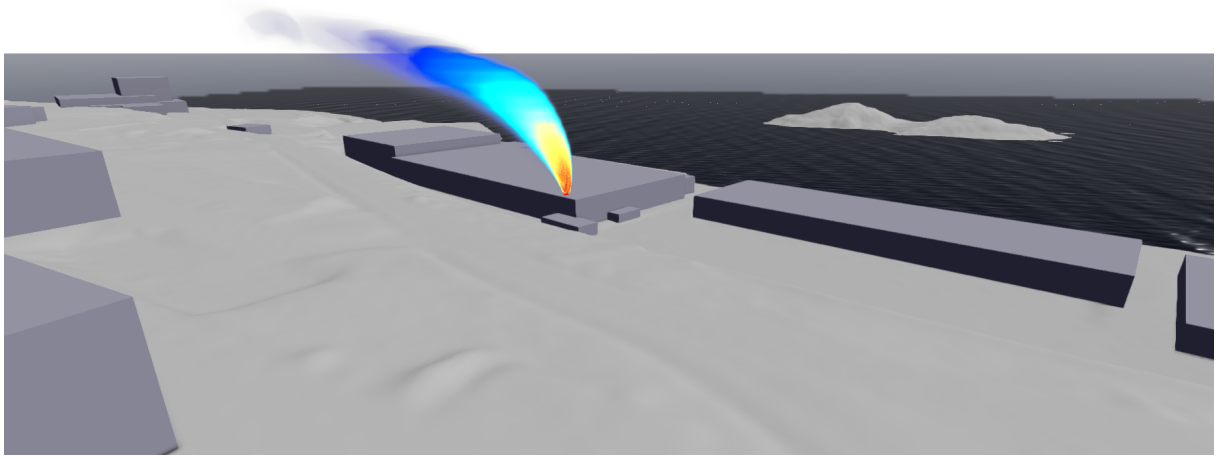

Figure 4.13: Three-dimensional plot showing the gas plume with concentration above 100 mg/m^3 when the release is moved to the roof of the facility, showing the dilution of the plume, viewed from SE. Wind from E-SE at 2.5 m/s.

Temperature

As the outside temperature can vary substantially, an analysis was completed with emphasis on this. Knowing that the temperature has an impact on whether a gas is categorized as a heavy or light gas, an interval of 0°C to 20°C was examined.

By varying the temperature, very little differences is seen in the extent of the dispersion. The overall extent of the three simulations differ only slightly, where only a minor shift of the cloud in the z-direction is experienced. A higher temperature shows more gas at a higher z-level, and thereby, also a slight increase in the concentrations at higher z-levels is seen.

As the gas is released with a temperature of 20°C, the lower outside temperature of both 0°C and 10°C should cool the gas slightly, increasing its density and reducing the buoyancy. Figure 4.14 illustrates just that. In the figure, the concentration development for three monitor points with constant x- and y-coordinate, and increasing z-coordinates, for the three simulations is shown, with 0°C on the left, 10°C in the middle and 20°C to the right. The concentration at the same monitor points decrease as the temperature also decrease, where °C and 10°C differ more than 10°C and 20°C.

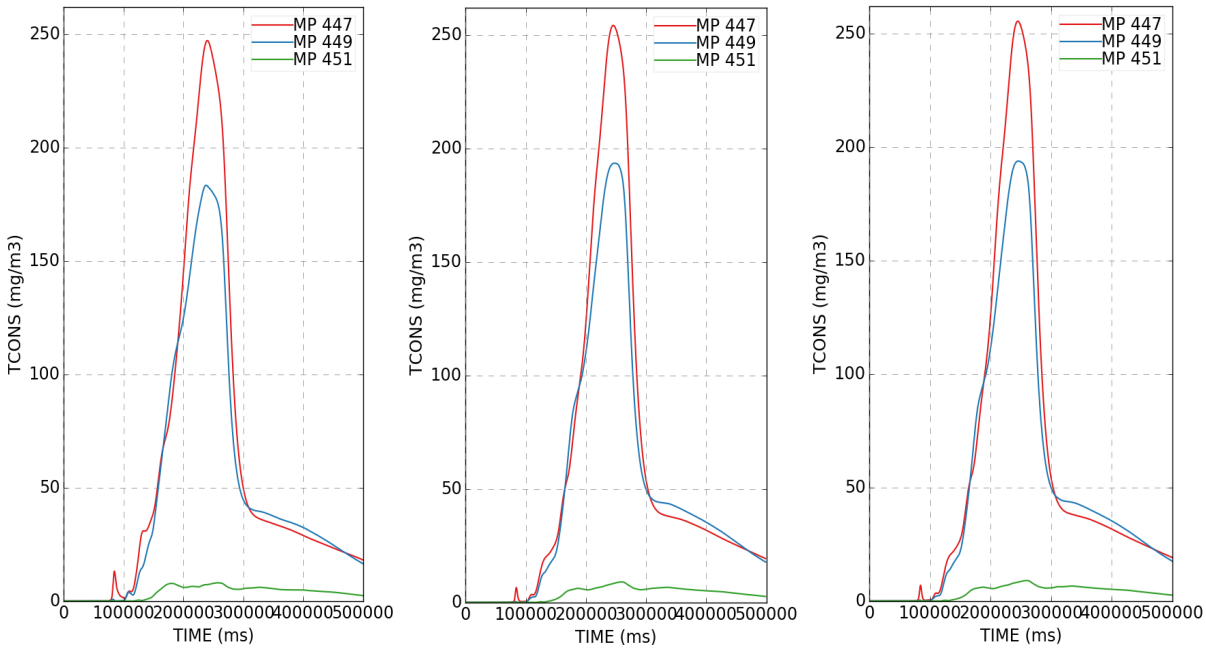

(a) 0°C **(b)** 10°C **(c)** 20°C

Figure 4.14: Concentration of ammonia measured at three different monitor points with constant x- and y-coordinate, and increasing z-levels, at (a) 0°C, (b) 10°C, which all the simulations were run with, and (c) 20°C.

As the lowest temperature examined is already more than 30°C above the boiling point the biggest variations in density has probably already been overcome. Thereby, if the temperatures differed more, or was closer to the boiling point, maybe larger differences would be experienced. Since only slight differences is seen, it is recognized that the assumed outside temperature of 10°C provides valid results, and that the extent of dispersion is independent of the temperature interval investigated here.

4.3 Uncertainties

Stretching

An interesting fact observed when adjusting and enlarging the grid of one scenario, was that when the studied domain was enlarged to a certain size, while keeping the grid size constant, it resulted in a different dispersion pattern. Figure 4.15 show simulation 100017 with the wind from E-NE at 2.5 m/s, and with an increasing stretched domain. With an increasing stretched domain, the extent of the gas cloud is decreasing. The reason for this is that, as long as the grid parameters, such as cell size and maximum cell size, remains the same, the maximum cell size is encountered closer to the leak when the stretched domain is small. For a smaller domain, the gradual increase from the grid size in the core domain to the maximum cell size at the boundaries is greater than for a larger domain, as it has a smaller domain to make the transition in. Having in mind that FLACS reports the average concentration in an entire cell, it is clear why a smaller stretched domain display a larger extent.

Numerous of the simulations show gas dispersion closing in on the boundaries and should probably have been re-run with further stretching, as the boundaries might have affected the results. To make sure that the boundaries did not alter the results, an enormous area had to be studied, and the same area had to be applied to every simulations. However, to ensure that the area studied considered all wind directions, it would have culminated in an excessive amount of cells, and would not be practically possible within the time limit for this thesis.

Non-aligned objects

When setting up the geometry, the buildings were placed in positions corresponding to their actual positions in the terrain. Thereby, they were not aligned to the x-, y- or z-axis, a fact that the user manual does not recommend. When opposing this recommendation, listed consequences include leaking of gas into unwanted and unlikely places, and enhanced leak areas.

The mentioned effect is in fact observed, where ammonia is found to be leaking into buildings, and as a repercussion the dispersion at times took an unexpected path, which might have affected the outcome. As previously mentioned, this possible consequence was ignored to ensure a realistic replica of the area.

Unsuccessful pool simulations

As the pool simulations were unsuccessful, it was decided to assume that all 750 kg that is contained, is released, evaporates and is ventilated out into the surroundings.

The facility has alarm systems and gas detectors which are expected to go off as a release takes place. With this in mind, the scenarios studied here might have all been worst-case scenarios, as the total amount of 750 could have been less had it been stopped premature.

Inconsistent grid size

Due to some scenarios requiring several enlargements of the domain, the grid size had to be adjusted and enlarged as well. Where it was justifiable considering the amount of grid cells, the original grid size was kept. Hence, two types of grid with different max size is invoked in this thesis. With the enlarged grid size, a slight overestimation in these is expected, and the two grid sizes might not be fully comparable. Two of the simulations having to have its grid cells enlarged was simulation 100027 and 100011, which showed the greatest extent. Even though the grid

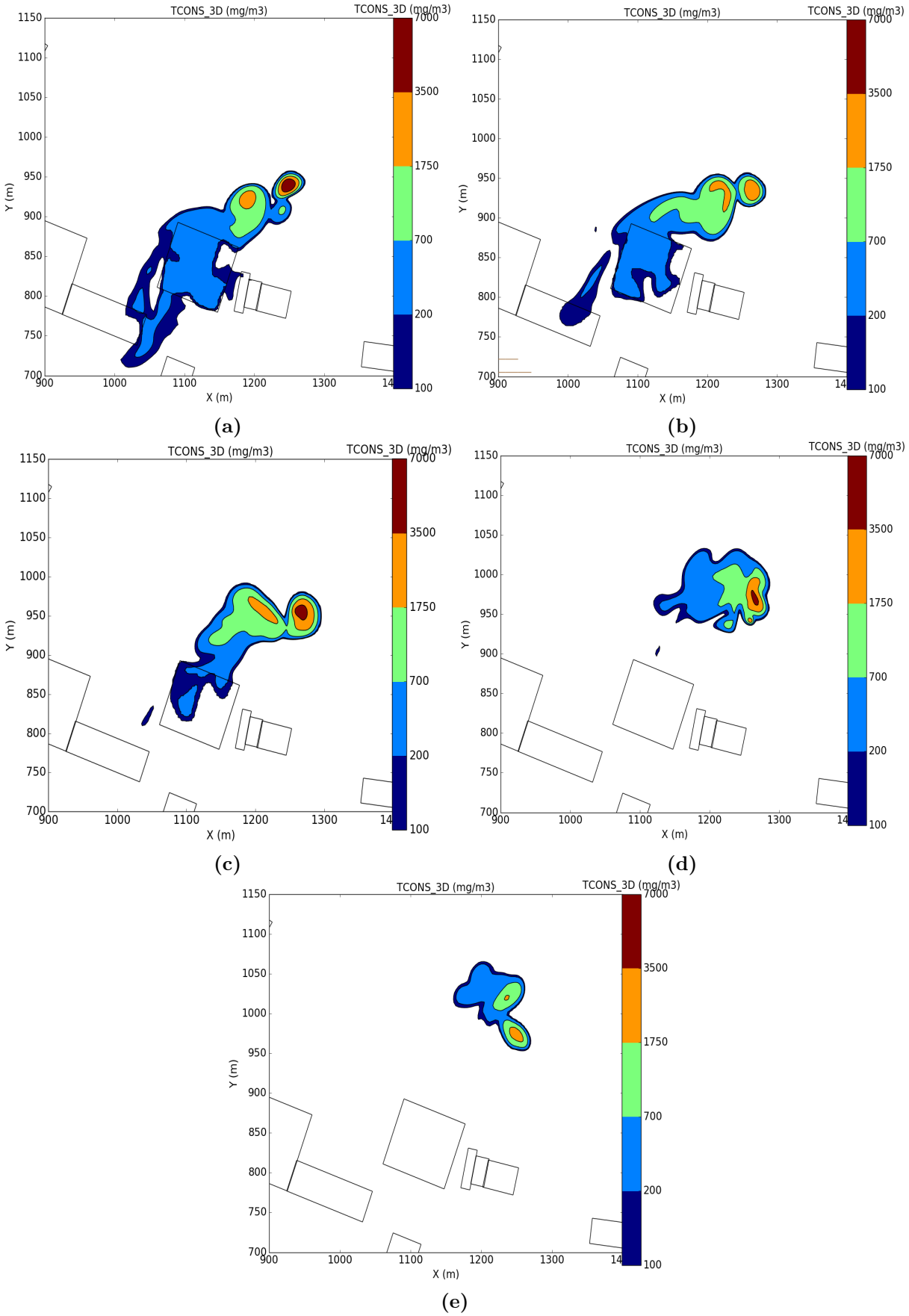

Figure 4.15: Dispersion of ammonia with the wind entering from E-NE at 2.5 m/s, shown with five different stretched grids. The stretching increases in size from (a) to (e), and display a decreasing extent with an increasing stretched domain.

size probably brought with it an overestimated extent, the gap from this scenario to the second most extensive scenario, was definitely larger than the overestimation probably experienced. All simulations should have been run with the same grid, as comparing simulations with different grids can be faulty.

Gas composition

When setting up the scenarios, the gas composition is chosen for the whole scenario, and is not possible to vary during. Taking the full case description into account, the concentration profile of the leak is expected to fluctuate, which the code is not mature enough to handle yet.

The leak setup only examined constant flows of ammonia, and the results could have differed if a leak with a varying concentration was added.

Sensitivities

When completing the sensitivities, they were only completed on one selected simulation. Therefore, the conclusion in the sensitivity analysis is based on one wind direction with one wind speed only. To ensure the viability of the several analysis completed, they should have been completed for the full set of simulations. The simulations greatly differ in wind characteristics, and combined with the geometry, it is not certain that the remarks concluded with here, is valid for the full set.

Buildings

Since the attempt of overlapping *.dem*-files, containing the terrain, with the *.dgn*-files, containing all objects such as buildings, was not successful, it had to be done manually. As this was a very time consuming task, only a fraction ended up being added to the terrain. It has previously been shown that buildings, and objects in general, contribute to mixing of the gas, and the missing objects not added might have played a role in affecting the dispersion. It was seen that in some locations, the gas was slowed down and even stopped completely. Thereby, providing a complete replica of the area would at least ensure that the missing objects did not affect the results.

Chapter 5

Conclusion

The dispersion of ammonia gas in an industrial area at different wind speeds and wind directions has been studied using the CFD tool FLACS. The major discoveries are listed below.

Looking at the different wind directions, dispersion scenarios with substantially different extent and hazard potential is obtained. Due to the location of the facility, and that the most common directions enters from the southern directions between E-SE and W-SW, only four out of the 12 most common winds are categorized as a category 2 dispersion, extending more than 600 meter.

Effect of grid size
Lowering the grid size below a uniform grid of 1.25 without a maximum cell size, reduces the apparent overestimation of the extent.

Refining the grid raises the concentrations in the z-direction somewhat, while the far-field concentrations are hardly affected. The refined jet shows a higher resolution and concentration close to the leak, due to the smaller cells, but this effect diminishes as the distance from the leak increases.

Effect of leak setup
For this geometry and these conditions, the way the leak is set up has only a modest impact on the results. The initial development differ some, where a high mass flow develops quicker, but the lower mass flow quickly catches up and attains the same shape and extent.

Effect of varying conditions

- Implementing Pasquill classes D, E or F has minor effects on the dispersion itself. However, the overall shape and tendencies of the cloud is affected, where using the mentioned classes reduce the instabilities of the cloud and limits the fluctuating tendencies seen when a class is not implemented.
- Comparing an unobstructed dispersion with its obstructed counterpart show the turbulent effects arising when obstacles are present. With buildings present, the cloud is attained in the leak location before the wind manages to release it, and ends up dispersing further than the unobstructed scenario.
- Elevation of the leak results in a quicker dilution and the buoyant plume hardly affects any areas.
- Lowering the outside temperature that the gas, at 20°C, is released into, from 10°C to 0° does not have any noticeable effect. However, when the temperature is raised to 20°C, slightly higher concentrations at higher z-levels is experienced. This indicates that the gas is slightly cooled when released into the original temperature of 10°C.

5.1 Suggestions for further work

First, effort needs to be put in to determine the correct set of variables used to define ammonia in the pool model in FLACS. This to make ammonia a standard fluid for the model, and would exclude human error introduced when a user defines its own species.

Second, obtaining a full picture as to how gas will disperse in the current area, all combinations of wind speeds and direction, independent of frequency should be examined. Also, to ensure the viability of these results, a large enough domain should be determined and implemented on all the simulations to minimize the effect of the boundaries.

Bibliography

[1] NRK. *En død etter ammoniakkeksplosjon.* [Online]. Available: https://www.nrk.no/vestfold/en-dod-etter-ammoniakkeksplosjon-1.272219 (Accessed: 02.01.2018), July 2002.

[2] ABC NEWS. *Ammonia leak China caused by detached pipe cap.* [Online]. Available: http://www.abc.net.au/news/2013-09-02/an-china-ammonia-deaths-caused-by-detatched-cap/4928574 (Accessed: 22.03.2018).

[3] W. Greulich and O. Hansen. "Quantitative Risk Analyses of Untreated, Vertical Pressure Relief Venting Using a Computational Fluid Dynamics Simulation". International Institute of Ammonia Refrigeration's Industrial Refrigeration Conference & Exhibition. Orlando, FL, March 2016.

[4] F. Gavelli, S. G. Davis, M. Ichard, and O. R. Hansen. "CFD Simulation of Gas Dispersion from Large-Scale Toxic Chemical Releases in Complex Environments". Texas City, TX, October 2011.

[5] F. Gavelli, M. Ichard, S. Davis, and O. R. Hansen. *"CFD simulations of the Jack Rabbit ammonia and chlorine release experiments using FLACS".* [Online]. https://ams.confex.com/ams/91Annual/webprogram/Paper186588.html (Accessed: 02.04.2018), January 2011.

[6] D. P. Storwold Jr, J. C. Pace, and S. B. Fox. "Extended Abstract For the Jack Rabbit Test Program Trial Summary". 2011.

[7] International Institute of Ammonia Refrigeration. *Ammonia Data Book.* International Institute of Ammonia Refrigeration, 2nd edition, 2008.

[8] US Department of Health and Human Services. "Toxicological Profile for Ammonia". Technical report, 2004.

[9] The National Institute for Occupational Safety and Health (NIOSH). *Immediately Dangerous to Life or Health Concentrations (IDLH): Ammonia.* [Online]. Available: https://www.cdc.gov/niosh/idlh/7664417.html (Accessed 16.01.2018).

[10] Committee on Acute Exposure Guideline Levels. *Acute Exposure Guideline Levels for Selected Airborne Chemicals: Vol. 6.* National Academy Press (US), Washington, D.C, 2008.

[11] Encyclopedia Britannica. *Haber-Bosch Process.* [Online]. Available: https://www.britannica.com/technology/Haber-Bosch-process (Accessed: 08.12.2017).

[12] U.S. Geological Survey and U.S. Department of the Interior. *Mineral Commodity Summaries 2017.* [Online]. Available: https:/minerals.usgs.gov/minerals/pubs/mcs/2017/mcs2017.pdf (Accessed: 05.12.2017), 2017.

[13] A. Afif, N. Radenahmad, Q. Cheok, S. Shams, J. H. Kim, and A. K. Azad. "Ammonia-Fed Fuel Cells: a Comprehensive Review". *Renewable and Sustainable Energy Reviews*, 60(Supplement C):822–835, 2016.

[14] M. I. Hegglin, D. W. Fahey, M. McFarland, S. A. Montzka, and E. R. Nash. "Twenty Questions and Answers About the Ozone Layer: 2014 Update. Scientific Assessment of Ozone Depletion". Technical report, World Meteorological Organization, Geneva, Switzerland, 2015.

[15] İ. Dinçer. *Refrigeration Systems and Applications*. Wiley, Chichester, West Sussex, U.K., 2nd edition, 2010.

[16] S. M. Grannell, D. N. Assanis, S. V. Bohac, and D. E. Gillespie. "The Fuel Mix Limits and Efficiency of a Stoichiometric, Ammonia, and Gasoline Dual Fueled Spark Ignition Engine". *Journal of Engineering for Gas Turbines and Power*, 130(4), April 2008.

[17] S. Frigo and R. Gentili. "Analysis of the Behaviour of a 4-stroke Si-Engine Fuelled with Ammonia and Hydrogen". *International Journal of Hydrogen Energy*, 38(3):1607–1615, February 2013.

[18] A. Klerke, C. H. Christensen, J. K. Nørskov, and T. Vegge. "Ammonia for Hydrogen Storage: Challenges and Opportunities". *Journal of Materials Chemistry*, 18(20):2304–2310, 2008.

[19] Sir D. Brewster, R. Taylor, Sir R. Kane, W. Francis, and J. Tyndall. *The London, Edinburgh and Dublin Philosophical Magazine and Journal of Science*. London, 1856.

[20] S. Wang. *Handbook of Air Conditioning and Refrigeration*. McGraw-Hill handbooks. McGraw-Hill, New York, 2. ed edition, 2001.

[21] S. Lees. *Lees' Loss Prevention in the Process Industries: Hazard Identification, Assessment and Control*. Elsevier Science, Oxford, United States, 4th edition, 2012.

[22] *Dispersion - definition of dispersion in English / Oxford Dictionaries*. [Online]. Available: https://en.oxforddictionaries.com/definition/dispersion (Accessed 04.04.2018).

[23] E. J. List. "Turbulent Jets and Plumes". *Annual Review of Fluid Mechanics*, 14(1):189–212, 1982.

[24] Gexcon AS. *FLACS v10.6 User's manual*. Gexcon AS, 2017.

[25] J. D. Anderson Jr. *Computational Fluid Dynamics*. McGraw-Hill Education, New York, 1st edition, February 1995.

[26] W. McCabe, J. Smith, and P. Harriott. *Unit Operations of Chemical Engineering*. McGraw-Hill Education, Boston, MA, 7th edition, 2004.

[27] J. Warnatz, U. Maas, and R. Dibble. *Combustion: Physical and Chemical Fundamentals, Modeling and Simulation, Experiments, Pollutant Formation*. Springer Berlin Heidelberg, Berlin, Heidelberg, 4th edition, 2006.

[28] O. R. Hansen, F. Gavelli, M. Ichard, and S. G. Davis. "Validation of FLACS Against Experimental Data Sets From The Model Evaluation Database For LNG Vapor Dispersion". *Journal of Loss Prevention in the Process Industries*, 23(6):857–877, November 2010.

[29] S. R Hanna, O. R. Hansen, and S. Dharmavaram. "FLACS CFD Air Quality Model Performance Evaluation with Kit Fox, MUST, Prairie Grass, and EMU Observations". *Atmospheric Environment*, 38(28):4675–4687, September 2004.

[30] S. R. Hanna, M. J. Brown, F. E. Camelli, S. T. Chan, W. J. Coirier, O. R. Hansen, A. H. Huber, S. Kim, and R. M. Reynolds. "Detailed Simulations of Atmospheric Flow and Dis-

persion in Downtown Manhattan: An Application of Five Computational Fluid Dynamics Models". *Bulletin of the American Meteorological Society*, 87(12):1713–1726, December 2006.

[31] Gexcon AS. *FLACS v10.7 User's manual*. Gexcon AS, 2017.

[32] National Institute of Standards and Technology Technology. *Ammonia NIST Chemistry WebBook*. [Online]. Available: https://webbook.nist.gov/cgi/cbook.cgi?ID=C7664417 (Accessed 06.04.2018).

[33] Wikipedia. *Ammonia (data page)*. [Online]. Available: https://en.wikipedia.org/w/index.php?title=Ammonia_(data_page)&oldid=830507559 (Accessed: 11.04.2018).

Appendices

Appendix A

Parameters for defining ammonia as a species for pool simulations

The full list of parameters involved in defining ammonia as a species for pool simulations is listed below. Others parameters, such as parameters regarding laminar burning velocity and its dependency on different variables, are needed to define a species, but for ammonia these are set to zero. The table below lists the parameters that are given a value different from zero.

Table A.1: The input variables to define ammonia as a species for pool simulations in FLACS. Several variables are not included in this table, but is still required to define ammonia as a species. The value of these were set to 0, and include variables such as OXY, the number of moles O_2 in 1 mole of ammonia.

Description	Value
Molecular weight, W_{FUEL}	17.030 g/mol
Liquid density, L_{DENS}	681.97 kg/m^3
First constant for the calculation of specific enthalpy of gaseous ammonia, A_{ENT}	1698.0 J/(kg·K)
Second constant for the calculation of specific enthalpy of gaseous ammonia, B_{ENT}	1.6462 J/(kg·K^2)
Third constant for the calculation of specific enthalpy of gaseous ammonia, D_{ENT}	-1103300 J/kg
First constant for the calculation of specific enthalpy of liquid ammonia, A_{LENT}	3102.8 J/(kg·K)
Second constant for the calculation of specific enthalpy of liquid ammonia. B_{LENT}	5.6278 J/(kg·K^1)
Third constant for the calculation of specific enthalpy of liquid ammonia, D_{LENT}	714040 J/kg
First constant for the calculation of surface tension between the liquid and the gas, A_{SIGMA}	0.087600 N/m
Second constant for the calculation of surface tension between the liquid and the gas, B_{SIGMA}	-0.00022265 N/(m·K)
First constant for the calculation of vapour pressure, A_{VAPPR}	22.641 N/m^2
Second constant for the calculation of vapour pressure, B_{VAPPR}	2501.1 N/(m^2·K)
Third constant for the calculation of vapour pressure, D_{VAPPR}	-15.000 K
First constant for the calculation of viscosity of liquid ammonia, $VISC_B$	359.22
Second constant for the calculation of viscosity of liquid ammonia, $VISC_{TO}$	70.546
First constant for the calculation of viscosity of gaseous ammonia, $VISC_{GA}$	-0.0000010832 (N·s)/m^2
Second constant for the calculation of viscosity of gaseous ammonia, $VISC_{GB}$	0.000000037855 (N·s)/(m^2·K)
First constant for the calculation of thermal conductivity of gaseous ammonia, $COND_{GA}$	-0.013789 W/(m·K)
Second constant for the calculation of thermal conductivity of gaseous ammonia, $COND_{GB}$	0.00013417 W/(m·K^2)
First constant for the calculation of thermal conductivity of liquid ammonia, $COND_{LA}$	1.4956 W/(m·K)
Second constant for the calculation of thermal conductivity of liquid ammonia, $COND_{LB}$	-0.34636 W/(m·K^{-2})
Critical temperature, T_{CRIT}	405.4 K
Critical pressure, P_{CRIT}	11333 Pa

Appendix B

Calculating the enthalpy constants

The starting point for the calculations is a polynomial form of the Shomate equation for heat capacity, which can be written as [32]:

$$C_p = A + B \cdot t + C \cdot t^2 + D \cdot t^3 + \frac{E}{t^2}, \tag{B.1}$$

where t is the temperature in Kelvin divided by 1000, and A, B, C, D and E are all constants, whose numerical values are listed in table B.1. The constants are valid between 298 and 1400 K, which is a too high temperature interval compared to that which ammonia is exposed to in this thesis. However, the constants are still applied due to the lack of other data.

Table B.1: Constants and their numerical values used in the calculation of the heat capacity of ammonia in its gaseous state, found in the NIST databook [32].

Variable	Value
A	19.99563
B	49.77119
C	-15.37599
D	1.921168
E	0.189174
F	-53.30667

Using equation (B.1), the heat capacities of the gaseous phase is calculated at 173.15 and 273.15 K to provide a basis for further calculations. As $dh = C_p dT$ at constant pressure, the relation used by FLACS to calculate the heat capacity is found by differentiating equation (3.1). This gives:

$$C_p = A_{ENT} + B_{ENT} \cdot T, \tag{B.2}$$

where the T is temperature in Kelvin and A_{ENT} and B_{ENT} is the first and second enthalpy constant, respectively. Equation (B.2) is a linear equation and B_{ENT} can be approximated by looking at it as the slope of the heat capacity and is determined using the relation:

$$B_{ENT} = \frac{C_{p,\ 273.15\ \mathrm{K}} - C_{p,\ 173.15\ \mathrm{K}}}{(273.15 - 173.15)K} = 5.46 \cdot 10^{-3} J/(mol \cdot K^2)$$

where the heat capacities calculated in equation (B.1) is used as input. A_{ENT} is found by rearranging equation (B.2), and is the value leading to the correct heat capacity at a given temperature when B_{ENT} is implemented. Data at T = 173.15 K is used to calculate A_{ENT}:

$$A_{ENT} = C_p - B_{ENT} \cdot T = 34.47231 - 5.46 \cdot 10^{-3} \cdot 173.15K = 33.53$$

Remaining is the third constants, D_{ENT}. Two more equations are needed for the calculation of the last constant. First, the equation for standard enthalpy is used [32]:

$$h = A \cdot t + \frac{B \cdot t^2}{2} + \frac{C \cdot t^3}{3} + \frac{D \cdot t^4}{4} - \frac{E}{t} + F \tag{B.3}$$

where the constants A through F is the same as in table 3.1. Calculating the standard enthalpies at the same temperature as above leads to the last values needed for calculation of D_{ENT}. The final equation is the equation listed in the user manual for D_{ENT}:

$$D_{ENT} = A_{ENT} \cdot T + 0.5 B_{ENT} \cdot T^2 - h \tag{B.4}$$

Table B.2: Calculated heat capacity and standard enthalpy of the gaseous phase at two different temperatures using the variables in table B.1.

Temperature, T (K)	**Heat capacity, C_p (J/(mol·K))**	**Standard enthalpy, h (kJ/mol)**	**Standard enthalpy, h (J/kg)**
173.15	34.47231	-50.21705	$-2.94857 \cdot 10^6$
273.15	35.01804	-46.78247	$-2.74690 \cdot 10^6$

For the liquid phase, a similar approach was used, only changing the temperature interval to 233.15 and 293.15 K. The two first constants, A_{LENT} and B_{LENT} were calculated in the exact same way as above, while D_{LENT} was calculated in a slightly different manner. The values for the liquid heat capacity was read of a graph, where heat capacity was plotted against the heat capacity for anhydrous liquid ammonia [33].

To determine the last variable, D_{LENT}, the enthalpy of the liquid at a given temperature is needed. Using the enthalpy of vaporization, specified to 23.35 kJ/mol, or 1371070 J/kg [33], at the boiling point, the enthalpy of the liquid at this temperature is calculated. This is done by first rearranging equation (B.4) with respect to the standard enthalpy, and calculating the enthalpy of the gaseous phase by implementing the new, calculated variables as seen table B.4. When this is done, the enthalpy of the liquid is establish by subtracting the enthalpy of vaporaization from the enthalpy of the gaseous phase. The calculated enthalpy of the liquid phase is used to calculate D_{LENT}, by the same equation as D_{ENT}, equation (B.4). Table B.3 list the old values and the proposed new values for the constants.

Table B.3: The old and new, proposed values for the two sets of enthalpy constants used in specification of ammonia in pool simulations.

Constant	**Old value**	**Proposed new value**
A_{ENT}	1698 J/(kg · K)	1968.6 J/(kg · K)
B_{ENT}	1.6462 J/(kg · K^2)	0.320433 J/(kg · K^2)
D_{ENT}	-1103300 J/(kg · K)	3294236 J/(kg · K)
A_{LENT}	3102.8 J/(kg · K)	2948.113 J/(kg · K)
B_{LENT}	5.6278 J/(kg · K^2)	6.067545 J/(kg · K^2)
D_{LENT}	714040 J/(kg · K)	5073914 J/(kg · K)

Appendix C

Wind data

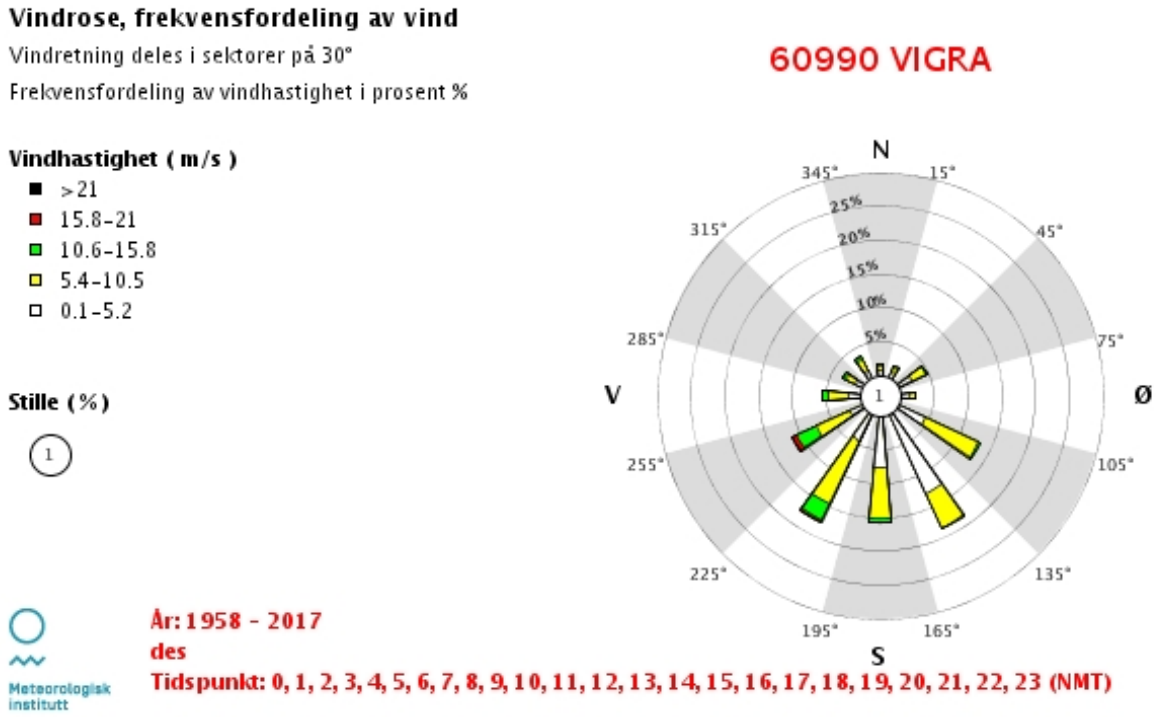

Figure C.1: Wind rose showing the relative frequencies of wind directions and wind speeds from the weather station '60990 Vigra', used to chose the wind speeds and directions examined in this thesis. The wind rose is based on data from 1958 to 2005 and was made at 'eklima.met.no' the 21st of march 2018.

I perioden 01.07.1958 - 31.05.2005 er data ved hovedtermin benyttet, i perioden 01.06.2005 - 31.12.2017 er timevise data benyttet

60990 Relativ frekvens (%) av observasjoner for DD horisontalt og FF vertikalt. 01.07.1958 - 31.12.2017
des. Alle tilgjengelige timer

	DD	345	15	45	75	105	135	165	195	225	255	285	315	Variabel	Stille	Sum	Rel.fr.	Kum.fr.	Middel	St.av.
FF		14	44	74	104	134	164	194	224	254	284	314	344						DD	DD
<=	0,0														0,5	69	0,5	0,5		
0,1	5,2	0,6	0,7	2,2	1,4	4,3	13,0	7,7	4,3	2,0	1,7	1,1	1,2		0,0	5841	40,3	40,8		
5,4	10,5	0,9	0,9	2,2	0,9	8,8	5,5	7,4	10,3	5,5	3,0	1,4	1,7			7047	48,6	89,4		
10,6	15,8	0,2	0,2	0,3	0,0	0,3	0,1	0,6	2,8	3,0	0,9	0,5	0,6			1367	9,4	98,8		
15,8	21,0	0,0	0,0	0,0				0,0	0,2	0,7	0,1	0,0	0,0			148	1,0	99,9		
>	21,0								0,0	0,1	0,0	0,0				20	0,1	100,0		
Sum		243	258	677	341	1949	2704	2275	2549	1647	820	452	507		70	14492				
Rel.fr.		1,7	1,8	4,7	2,4	13,4	18,7	15,7	17,6	11,4	5,7	3,1	3,5		0,5		100,0			
Kum.fr.		1,7	3,5	8,1	10,5	23,9	42,6	58,3	75,9	87,2	92,9	96,0	99,5		100,0					
Middel	FF	6,5	6,4	5,9	4,8	6,2	4,6	5,6	7,6	9,2	7,3	7,1	7,0		0,0					
St.av.	FF	3,2	3,2	2,9	2,6	2,2	1,7	2,6	3,2	4,2	3,4	3,6	3,5		0,0					

Figure C.2: The relative frequencies of wind direction and wind speeds from the weather station '60990 Vigra' used to chose the wind speeds and directions examined in this thesis. The wind directions are divided into 30° intervals, and wind speeds in five intervals ranging from 0 m/s to $>$ 21 m/s. The table is based on data from 1958 to 2005 and was made at 'eklima.met.no' the 21st of march 2018.

Appendix D

Additional results: Dispersion plots

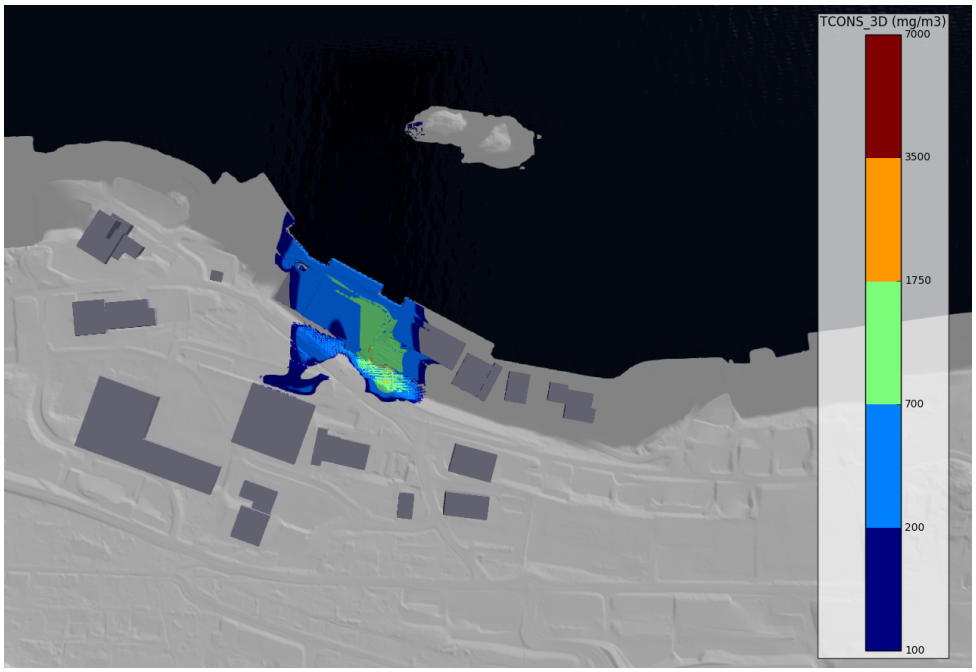

Figure D.1: Three-dimensional surface plot showing dispersion of ammonia gas with concentrations greater 100 mg/m^3 when the wind enters from S with a wind speed of 2.5 m/s, 410 seconds into the release.

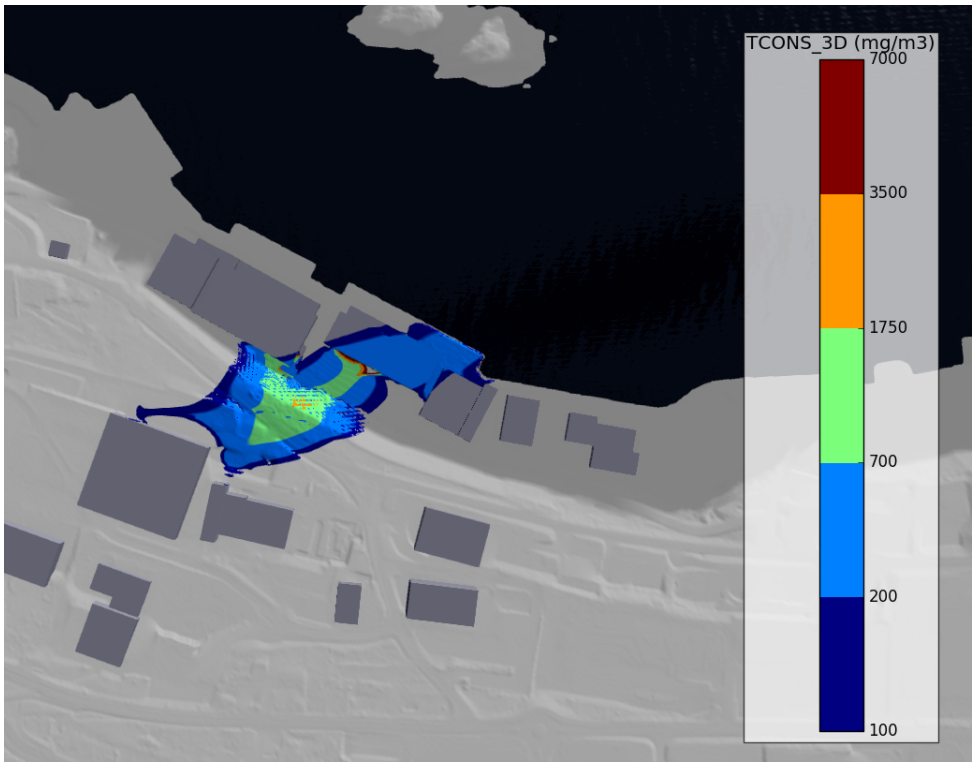

Figure D.2: Three-dimensional surface plot showing dispersion of ammonia gas with concentrations greater 100 mg/m^3 when the wind enters from W-SW with a wind speed of 7.5 m/s, 300 seconds into the release.

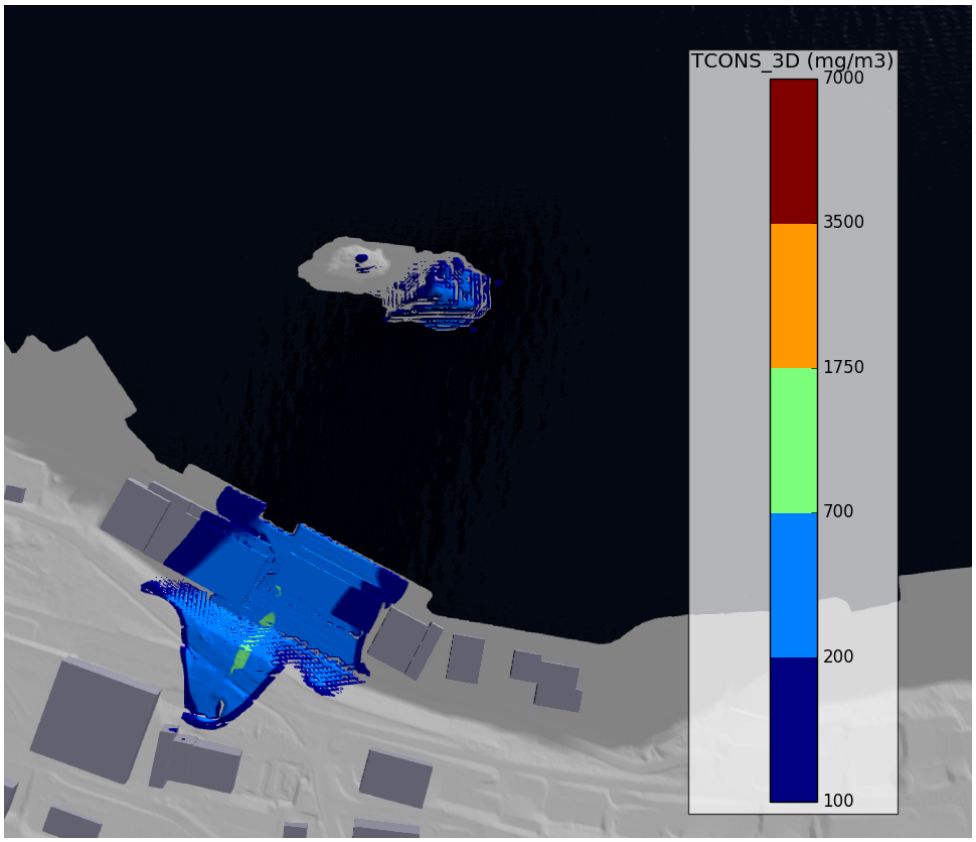

Figure D.3: Three-dimensional surface plot of dispersion of ammonia gas with concentration above 100 mg/m^3 when the wind enters from S-SW with a wind speed of 2.5 m/s, 490 seconds into the release.

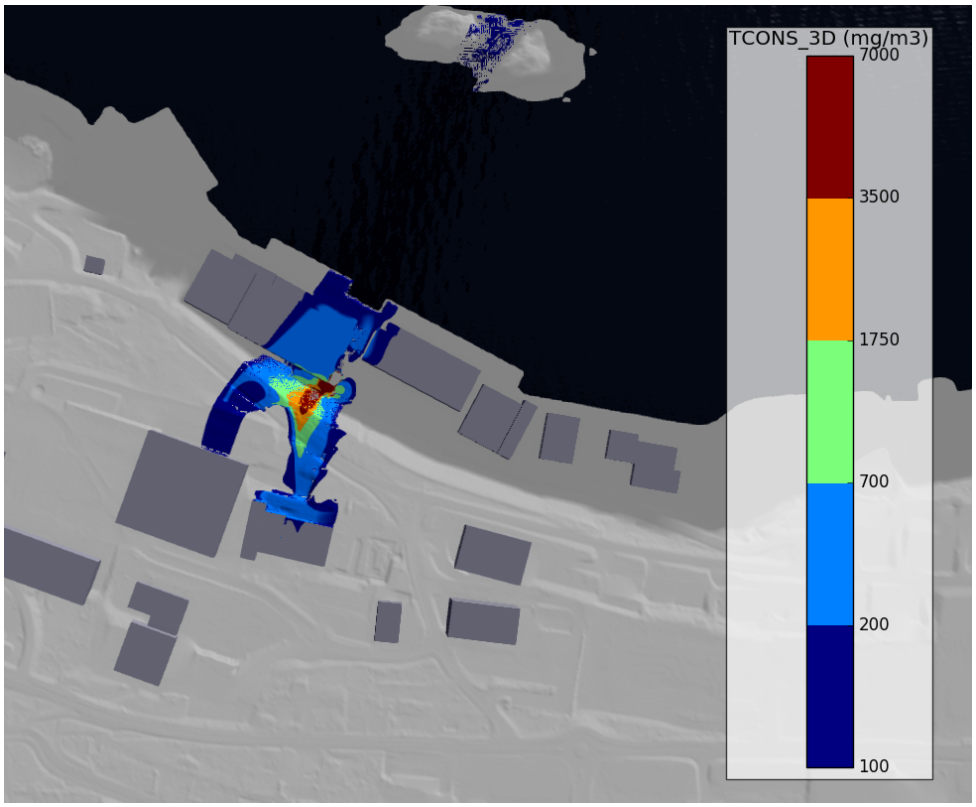

Figure D.4: Three-dimensional surface plot showing dispersion of ammonia gas with concentrations greater 100 mg/m^3 when the wind enters from S-SW with a wind speed of 7.5 m/s, 250 seconds into the release.

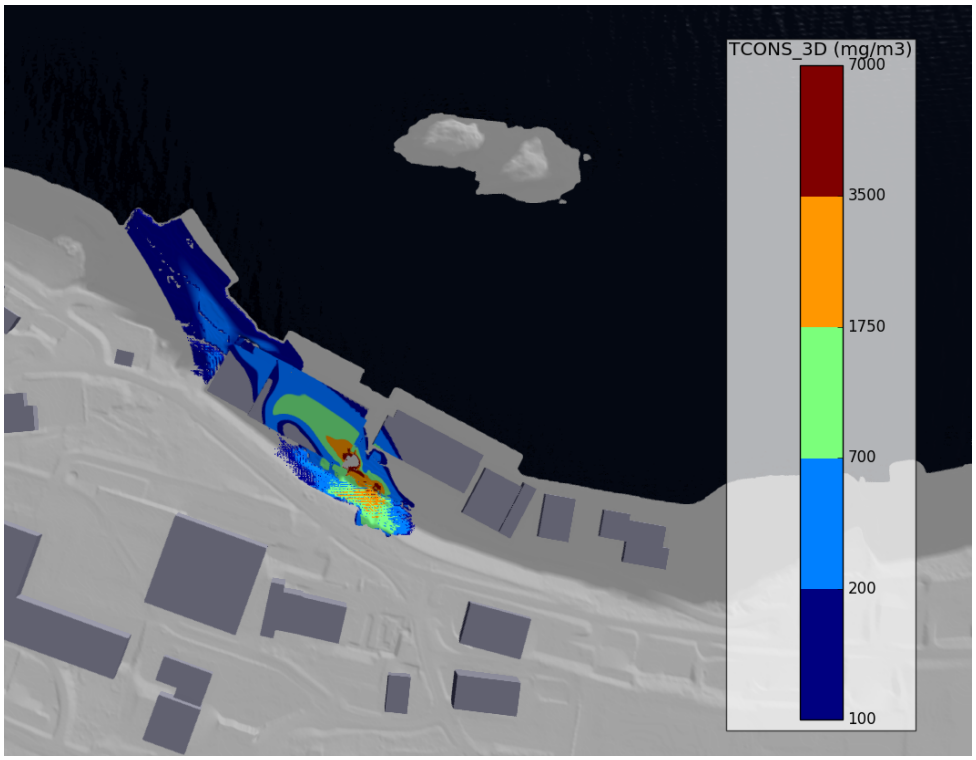

Figure D.5: Three-dimensional surface plot showing dispersion of ammonia gas with concentrations greater 100 mg/m^3 when the wind enters from S-SE with a wind speed of 7.5 m/s, 270 seconds into the release.

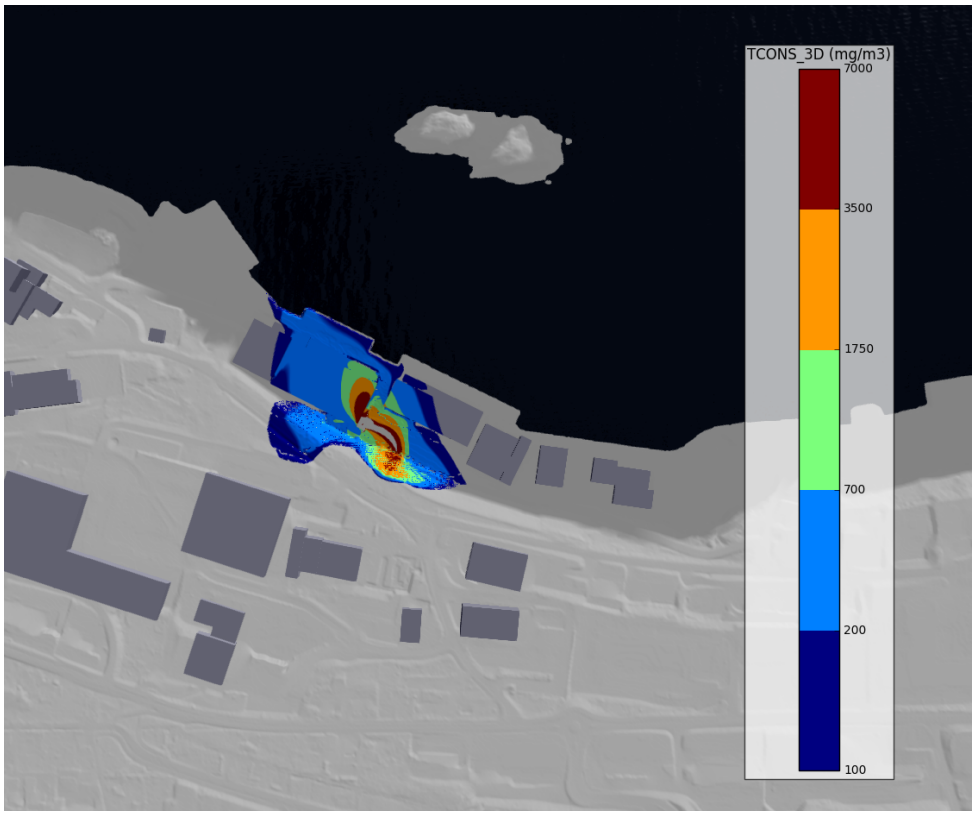

Figure D.6: Three-dimensional surface plot showing dispersion of ammonia gas with concentrations greater 100 mg/m^3 when the wind enters from S with a wind speed of 7.5 m/s, 180 seconds into the release.

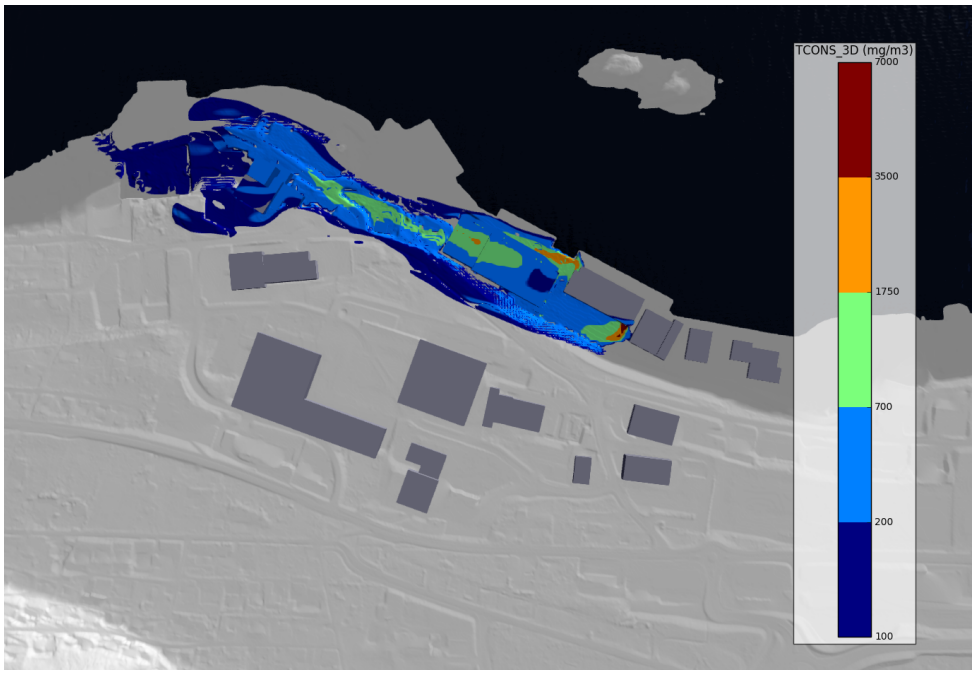

Figure D.7: Three-dimensional surface plot showing dispersion of ammonia gas with concentrations greater 100 mg/m^3 when the wind enters from E-SE with a wind speed of 2.5 m/s, 350 seconds into the release.

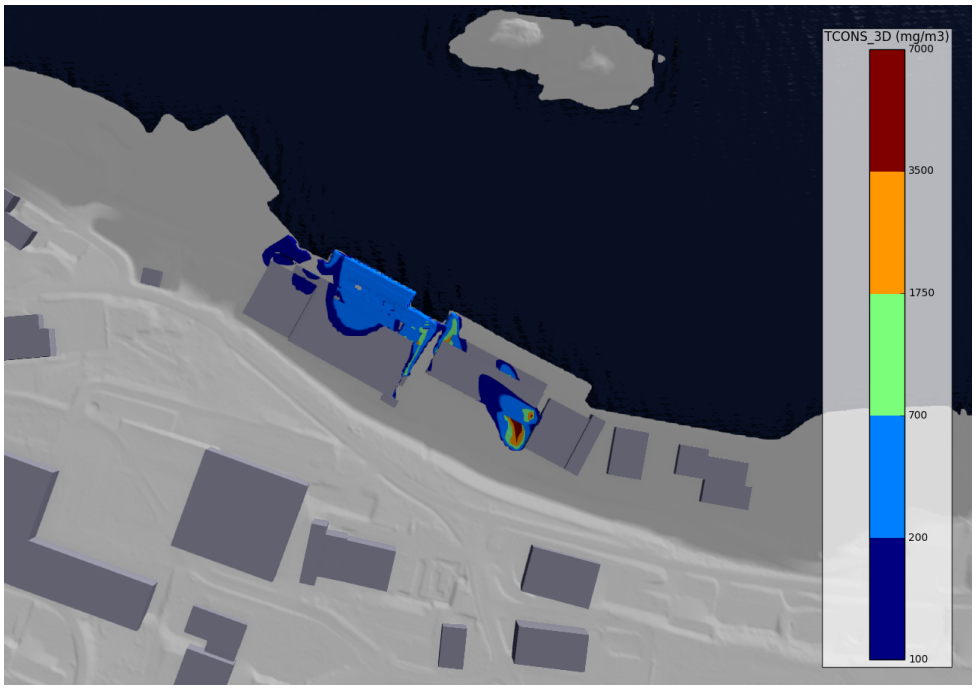

Figure D.8: Three-dimensional surface plot showing dispersion of ammonia gas with concentrations greater 100 mg/m^3 when the wind enters from E-NE with a wind speed of 2.5 m/s, 320 seconds into the release.

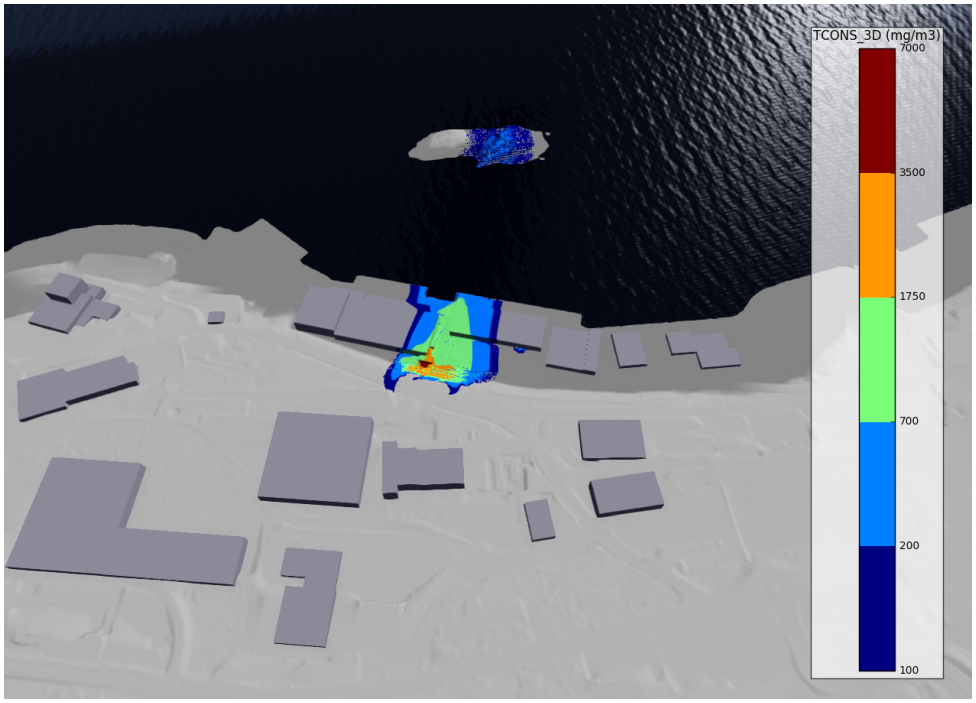

Figure D.9: Three-dimensional surface plot showing dispersion of ammonia gas with concentrations greater 100 mg/m^3 when the wind enters from S-SW with a wind speed of 12.5 m/s, 290 seconds into the release.

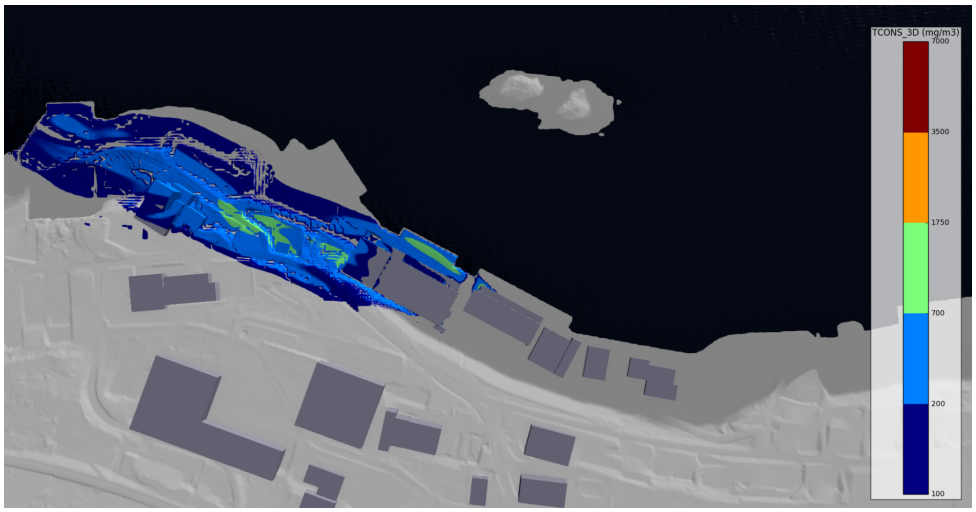

Figure D.10: Three-dimensional surface plot showing dispersion of ammonia gas with concentrations greater 100 mg/m^3 when the wind enters from S-SE with a wind speed of 2.5 m/s, 420 seconds into the release.

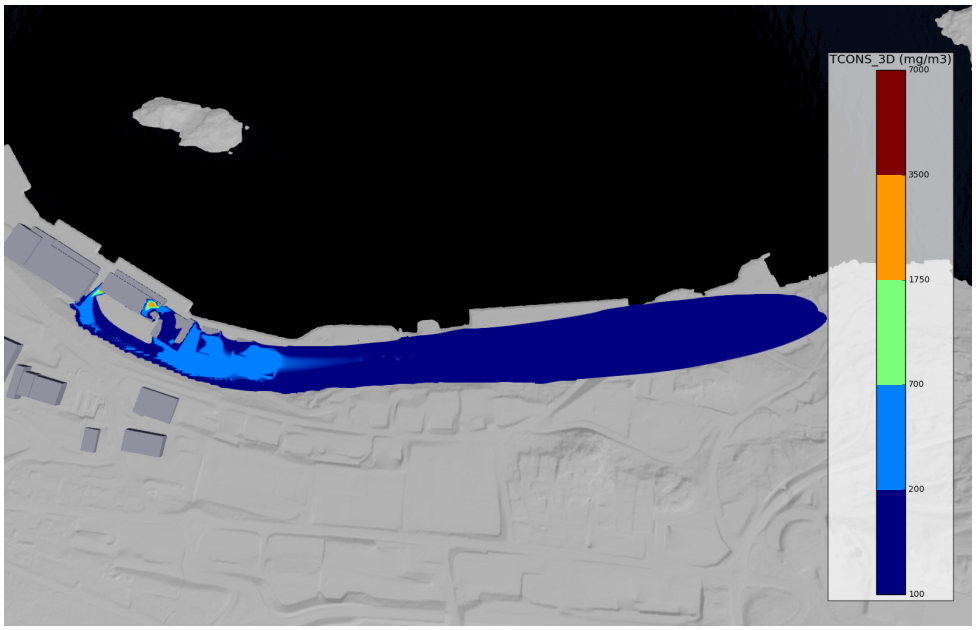

Figure D.11: Three-dimensional surface plot showing dispersion of ammonia gas with concentrations greater 100 mg/m^3 when the wind enters from W with a wind speed of 7.5 m/s, 420 seconds into the release

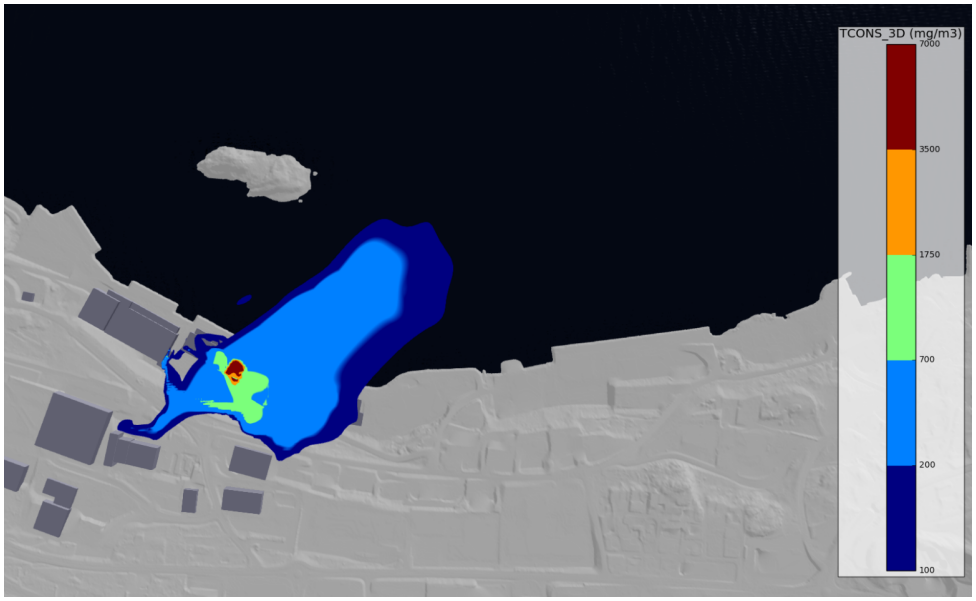

(a)

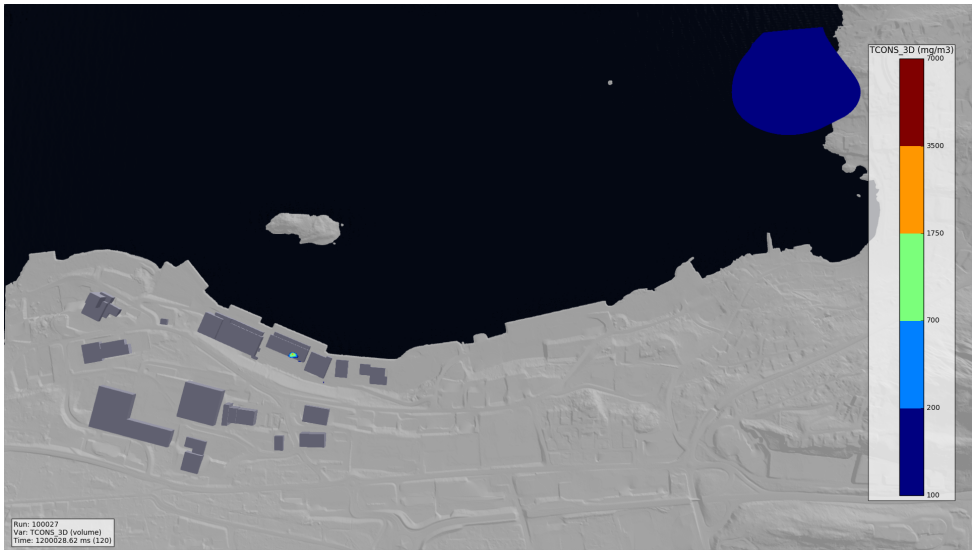

(b)

Figure D.12: Two-dimensional plot showing dispersion of ammonia gas with concentration above 100 mg/m^3 when the wind enters from W-SW with a wind speed of 2.5 m/s, at z = 1.5 and (a) 420 and (b) 1200 seconds into the release.